Journal of Sound and Vibration (1998) **215**(2), 343–379
Article No. 981637

AN EXPERIMENTALLY VERIFIED NON-LINEAR DAMPING MODEL FOR LARGE AMPLITUDE RANDOM VIBRATION OF A CLAMPED-CLAMPED BEAM

M. Ghanbari and J. F. Dunne

*School of Engineering, The University of Sussex, Falmer, Brighton, BN*1 9*QT, England*

(*Received* 2 *December* 1997, *and in final form* 30 *March* 1998)

An empirical non-linear damping model, for use with single-degree-of-freedom clamped-clamped beam vibrations driven by band-limited white noise, is calibrated by using large amplitude experimental measurements. To verify the model, two parameter estimation methods are initially tested on simulated data using (1) the state variable filter, and (2) a Markov based moment method—the moment method being preferred in this particular application. Model verification with real data, then proceeds by using moment based parameter estimation and finite element solutions of the stationary Fokker–Planck equation, where deliberate attempts have been made to avoid excitation of higher modes. By systematically building up from a simple linear to a three-term damping model, comparison between measurement and prediction, via the calibrated model, shows excellent agreement for probability density functions associated with the central beam displacement up to a normalized non-linear beam amplitude ratio = 7·0. But the subsequent comparisons of measured and predicted extreme value exceedance probabilities up to a maximum normalized amplitude ratio = 10·0, using the same calibrated SDOF model, shows significant differences, suggesting the occurrence of considerable non-linear coupling of beam vibrations. This finding would suggest, for the case of forced random vibration of a clamped-clamped beam, that a SDOF beam model is adequate for moderately large amplitude prediction but wholly inadequate at very large amplitudes.

1. INTRODUCTION

Large amplitude forced random vibration of clamped-clamped beams is important in several areas of structural dynamics, especially for prediction of high stress levels in aircraft panels exposed to high intensity acoustic loading. Although thermal effects may be crucial in some studies, isothermal models are still important and by no means fully understood. Large amplitude analysis of beams with *immovable* ends is initially complicated by "hardening" type geometric non-linearity which often proves too strong for linear (Euler–Bernoulli) theory, justifying use of the more general Woinowsky–Krieger equation [1] or use of nonlinear finite element models. The classical theory [1] can be usefully employed in free vibration studies by using several advanced non-linear analysis methods [2] although increasing emphasis is being placed on the FEM. In focusing discussion of this vast subject, it is initially helpful to consider separate topics of free and forced response prediction, beam damping, and combined acoustic-thermal loading.

Work on *free vibration* of nonlinear beams began with use of an elliptic integral [1] to obtain natural frequencies for pinned beams with *immovable* ends. Atluri [3] identified four main sources of non-linearity resulting respectively from (1) moderately large curvatures,

0022–460X/98/320343 + 37 $30.00/0

(2) longitudinal elastic forces and displacements, (3) longitudinal inertia, and (4) rotary inertia, confirming the effect of inertia for hinged beams as being of softening type. Mei [4] explained extraordinary hardening effects reported for simply supported (non-slender) beams with *immovable* ends, confirming that the effect of longitudinal displacement and inertia (ELDI) gives a reduction in non-linearity. Two further controversial points were examined by Singh *et al*. [5] to establish (i) whether axial strain should be included in the strain energy equation, and (ii) whether strain displacement can be linearized. It was shown that when axial strain is ignored, and strain displacement is linearized, a single harmonic solution via the Duffing equation, yields exactly the same natural frequency as the perturbation method, Rayleigh–Ritz, and elliptical integral when applied to corresponding dynamic models where neither assumptions are made and where a multiple harmonic solution is used. More recently Shi and Mei [6] have developed a finite element model including a non-linear strain–displacement relation to obtain modal equations for large amplitude beam motion. Their resulting system of equations can be reduced by using (linear) normal coordinates to obtain coupled Duffing-type equations (via a route considered much simpler than the classical Galerkin approach). Subsequent time-domain solution (with appropriate initial conditions) gives accurate natural frequencies and percentage participation from non-linear coupling, showing the number of degrees of freedom needed for increasing beam amplitudes. At normalized beam amplitudes >3, for example, at least two modes are considered needed for accurate frequency prediction. Lee *et al*. [7] extended this FEM to non-isotropic plates explaining how initial conditions should be chosen. Although the FEM looks set to grow in use, the accuracy of the classical Woinowsky-Krieger–Galerkin approach has recently been confirmed for free vibration of simply supported beams with *immovable* ends [8].

Forced vibration of non-linear beams has also received considerable attention, both for frequency response and stability analysis with harmonic excitation, and for response prediction with random forcing. Three early contributions include the work of Bennet and Eisley [9] using a 3-mode model via Galerkin's method to examine a damped beam with concentrated harmonic force, the one-mode approximation by Tseng and Dugundji [10] using Galerkin's method and harmonic balance to obtain experimentally observed sub- and super-harmonics for a clamped beam, and the work of Mei [11] using the matrix displacement approach for non-linear analysis. Busby and Weingarten also used discrete methods examining various non-linear beam problems including random response prediction [12] using the method of equivalent linearization. More recently Takahashi [13] has studied the stability of a harmonically excited clamped-clamped beam, also confirming experimentally observed phenomena. And in a detailed experimental study of a clamped beam with both harmonic and random excitation, Bennouna and White [14] showed that there is considerable reduction in fatigue life owing to axial strain caused by non-linear vibration. Mei and Decha-Umphai [15] confirmed, again for harmonically excited (non-slender) beams with *movable* ends, that non-linearity is indeed of softening type, and Benamar *et al*. [16] demonstrated that the curvature near the clamps of an harmonically excited clamped beam, depends strongly on amplitude, bending strain being a highly non-linear function of deflection. Recently Ribeiro and Petyt [17] have developed an hierarchical FEM specifically to include higher mode contributions and damping, without excessive increase in the number of DOF; this has been used mainly for stability and response analysis of clamped beams, but also to examine the influence of model order.

Accurate prediction of large amplitude forced vibration of non-linear beams is complicated by the need for good damping models, especially where several vibration modes are driven simultaneously by broad-band random excitation. Since beam damping levels are light, responses are critically controlled by the prevailing damping mechanism.

Damping synthesis is not yet possible owing to complex interaction (including hysteresis [18]) which prevents adequate separation into distinct components. Moreover, aerodynamic damping of random vibration (which may contribute a significant part of the total) cannot be accurately predicted by using classical fluid dynamics, so use of simpler empirical models is justified. Early work on large amplitude beam damping by Smith *et al*. [19] confirmed that linear damping in the Duffing equation was totally unsuitable. Subsequent use of linear-plus-quadratic model by Baker *et al*. [20], for free decay responses of a thin cantilever, has proved less useful in forced random vibration. A numerical study by Bandstra [21] examined prediction errors resulting from use of linearized damping for the models suggested in reference [20], concluding that none should in fact be linearized. More recently, in an attempt to explain experimentally observed broadening of the strain response peak and the increase in modal frequency of aircraft panels at high sound levels, Mei and Prasad [22] used three-term nonlinear damping in a Duffing equation for clamped-clamped beam vibrations showing that nonlinear damping contributes significantly to broadening of the response peak, and to changes in the maximum deflection, strain statistics and frequency for sound pressure levels >120 dB. In this study use of *linearized* damping led to the conclusions that (i) nonlinear damping has a profound effect on the fatigue life of panels above 120 dB, and (ii) more research on damping of random vibration is needed.

Combined thermal-acoustic loading has recently been included in forced analysis by a number of investigators including Chiang [23] and Wolfe [24]. Indeed Chen *et al*. [25] approached the combined loading problem for clamped beams using an FEM, model reduction, and statistical linearization to obtain (for the isothermal case) excellent agreement in predicted normalized beam displacements when using 1- and 4-mode models, but significantly less agreement when using a 1-mode model with FPK based predictions (this implies a fully nonlinear SDOF model should be adequate here for moderate amplitudes). But with combined thermal loading, there was excellent agreement between the 1-mode, 4-mode *and* the FPK based predictions (implying here that a linear SDOF model should be adequate).

In this paper we report large amplitude experimental measurements of clamped-clamped beam vibrations used to establish whether a modified three-term damping model is appropriate for use with a SDOF random vibration model. Two parameter estimation methods were initially tested with simulated data, and subsequent predictions, which form part of the verification, were obtained via appropriately matched finite element solutions of the stationary FPK equation. By including all combinations of damping terms to expose interactive behaviour, a gradual build-up to the specific three-term model was demonstrated at response amplitude marginal density level. Furthermore, extreme value predictions, which offer the most definitive verification of the same SDOF model are compared with experimental measurements to establish, for band-limited white noise excitation, the suitability of the model at very large amplitudes of vibration.

2. PREDICTION OF LARGE AMPLITUDE RESPONSE STATISTICS VIA A SDOF FORCED RANDOM VIBRATION MODEL

We briefly outline here the use of the classical nonlinear beam model, extracting from it—via Galerkin's method—a single-degree-of-freedom model along similar lines as for example in references [8, 10, 14, 22]. Attention will then turn to the choice of empirical nonlinear damping obtained as a modification to the three-term model used in reference [22], and the final part gives an overview of the prediction approach to marginal probability density functions and extreme value statistics.

Large amplitude vibrations of a clamped-clamped beam can be modelled by the Woinowsky-Krieger equation [1],

$$EI\frac{\partial^4 W(x,t)}{\partial x^4} - \frac{EA_B}{2L}\int_0^L \left(\frac{\partial W(x,t)}{\partial x}\right)^2 \mathrm{d}x \frac{\partial^2 W}{\partial x^2} + \rho A_B \frac{\partial^2 W(x,t)}{\partial t^2} = P(x,t), \tag{1}$$

upon assuming that rotary inertia and shear deflection are ignored, and that the beam of length L and elastic modulus EI, with transverse deflection $W(x, t)$, is subject to boundary conditions: $\partial W/\partial x = W = 0$ at $x = 0$ and $x = L$. Here, the initial tension is zero and the inhomogeneous forcing term $P(x, t)$ includes both a band-limited white noise source (concentrated at some point on the beam) plus all other external forces, such as damping. Of particular interest here is the central beam displacement $w = W(L/2, t)$, or more appropriately the normalized displacement ratio w/r which gives a measure of beam nonlinearity [1], where $r = \sqrt{I/A_b}$ (I is the second moment of area, and A_B is the beam sectional area).

If it is practically possible to construct a SDOF (discrete) beam vibration model from equation (1), at least by imposing appropriate upper and lower limits on the noise band-width, then this should allow an empirical damping model to be verified. Construction of a SDOF model from equation (1) is approached by assuming a single coordinate generalized beam displacement of the form

$$W(x,t) = \phi(x)z(t), \tag{2}$$

where $z(t)$ is an amplitude function (of time), and $\phi(x)$ is an assumed displacement shape function (of space). Substitution of equation (2) into equation (1) and application of Galerkin's method [22] gives

$$z(t)\int_0^L EI\frac{\partial^4\phi(x)}{\partial x^4}\phi(x)\,\mathrm{d}x - z^3(t)\int_0^L \left\{\frac{EA_B}{2L}\int_0^L \left(\frac{\partial\phi(x)}{\partial x}\right)^2 \mathrm{d}x \frac{\partial^2\phi(x)}{\partial x^2}\right\}\phi(x)\,\mathrm{d}x$$

$$+\ddot{z}(t)\int_0^L \rho A_B\phi(x)^2\,\mathrm{d}x = \int_0^L P(x,t)\phi(x)\,\mathrm{d}x. \tag{3}$$

This is equivalent to the undamped forced Duffing equation

$$\ddot{z}(t) + \omega_n^2 z(t)(1 + \gamma z^2(t)) = f(t), \tag{4}$$

where $f(t)$ is a form of generalized excitation and where the parameters ω_n^2 and $\gamma\omega_n^2$ are given as

$$\omega_n^2 = \frac{\displaystyle\int_0^L EI\frac{\partial^4\phi(x)}{\partial x^4}\phi(x)\,\mathrm{d}x}{\displaystyle\int_0^L \rho A_B\phi(x)^2\,\mathrm{d}x} \tag{5}$$

and

$$\gamma\omega_n^2 = \frac{-\int_0^L \left\{\frac{E}{2L}\int_0^L \left(\frac{\partial\phi(x)}{\partial x}\right)^2 \mathrm{d}x \, \frac{\partial^2\phi(x)}{\partial x^2}\right\}\phi(x)\,\mathrm{d}x}{\int_0^L \rho A_B \phi(x)^2\,\mathrm{d}x}. \tag{6}$$

Unfortunately the parameters ω_n^2 and $\gamma\omega_n^2$ given by equations (5) and (6) depend on the unknown displacement shape function $\phi(x)$, and this is one reason why there is interest in the use of large amplitude free vibration mode shapes since these may resemble the appropriate deflection shape function under particular forced conditions (such as for a centrally positioned harmonic force where, for reasons of symmetry, nonlinear coupling from a second mode for example, would not be expected [17]). Several approximate methods [2] can be used to obtain nonlinear free vibration mode shapes, for example via (i) postulating a time dependent solution with space dependent coefficients followed by use of the harmonic balance method to construct a nonlinear boundary value problem for the required coefficients, or (ii) using chosen space functions (e.g. linear mode shapes) followed by Galerkin's method to construct coupled nonlinear equations for the modal amplitude time functions, handled then by a perturbation technique or method of normal forms, and (iii) by generating normal modes directly from equation (1) by using the method of multiple scales. Unfortunately use of a single free vibration mode shape (even when ELDI is included) cannot possibly give consistent (stiffness) parameters under all forced vibration conditions because changes in the position of a concentrated load for example, would be expected to cause a change in the model parameters; equations (5) and (6) cannot take this into account. Also under experimentally forced conditions, when using for example an electromagnetic shaker, an unpredictably small but not insignificant part of the measured dynamic properties may be attributable to influences of the shaker [24]; obviously this information also cannot be included within equations (5) and (6). Moreover the whole question of the damping model, which is crucial for accurate response prediction, remains to be included in the model. But damping is a major source of difficulty [22] since this is made up from several nonlinear mechanisms either internal in origin (e.g. structural or material) or external (viscous, acoustic, dry friction, etc.). These energy losses occur at microscopic and macroscopic levels, and sometimes in the form of hysteresis. Suppose one considers just one component alone, such as derived from viscous fluid forces for example; these are particularly important for vibrating beams in air, and yet a good fluid drag model under random vibration conditions is not yet available. Much use has therefore been made of experimentally calibrated empirical models for both internal and fluid damping mechanisms for use with relatively simple equations of motion. The simplest form of damping is of course a linear model even though Bandstra [21] has demonstrated the adverse effect of replacing Coulomb, fluid drag, and structural damping models with an equivalent linear mechanism. To some extent this is borne out by the wide range of linear damping factors which seem to be used for beam vibrations. In reference [10], for example, a linear clamped-clamped beam damping factor of 0·6% critical was obtained from free decay tests. By contrast 1·9% critical clamped beam damping (which was rightfully reported with caution in reference [24]) was used in reference [17] to give amplitude predictions of around half the maximum obtained experimentally. And in reference [25], linear damping factors of 0·5% and 1% (for isothermal predictions) were compared with experimental measurements showing that normalized response predictions were bounded by these damping values. Clearly if damping is highly nonlinear, then accurate response amplitude prediction will not be possible when using linear loss factors.

In constructing a modified empirical beam damping model for use in a Duffing-type equation, motivation is initially drawn from reference [25] and from the partial success (at low intensities) of the model used by Smith *et al*. [19], in the form

$$C_1\dot{z} + \alpha_1 z^2\dot{z}, \tag{7}$$

which was used for predicting clamped-clamped beam vibrations excited by sinusoidal acoustic pressure. The success of this model would suggest this may actually form a good basis for a new model if an appropriate extension can be found. In fact the extension is derived here from the model used by Baker *et al*. [20], namely the well known empirical viscous damping model

$$C_1\dot{z} + \alpha_2\dot{z}|\dot{z}|, \tag{8}$$

which was very successful in modelling fluid damping of free decay responses of a thin cantilever beam. On combining expressions (7) and (8), a seemingly simple model follows. When this is inserted into the Duffing equation for a SDOF clamped-clamped beam undergoing large amplitude vibration, one obtains

$$\ddot{z} + C_1\dot{z} + \alpha_1\dot{z}z^2 + \alpha_2 z|\dot{z}| + \omega_n^2 z(1 + \gamma z^2) = f(t). \tag{9}$$

Contrast this type of damping with the three-term model of the form $c_1\dot{z} + c_2\dot{z}z^2 + c_3 z\dot{z}^2$ also used in a Duffing-type equation by Mei and Prasad [22] whose limitations for clamped-clamped beam vibrations were clearly identified based on predictions obtained with equivalent linearization. It would not be thought however that a seemingly subtle difference from this three-term model would have a major impact—but this is not the case as we will see in due course; in fact, all but the linear damping term in equation (9) seem to interact in an unexpectedly complex way. Now since the stiffness parameters given by equations (5) and (6) depend on the choice of displacement shape function, the only practical way to obtain all of the parameters (C_1, α_1, α_2, ω_n^2 and γ) is via direct calibration by using experimentally measured data, it being assumed that this data can be processed by a suitable parameter estimation technique. Fortunately one major advantage of modelling the forcing term as a white noise process is that specific non-linear techniques based on Markov process theory (via the FPK equation) can be used for obtaining theoretical predictions of certain response statistics, as well as forming the basis for one of the parameter estimation methods. The Markov approach to the statistics of interest, namely marginal density functions and extreme values, is now outlined briefly.

2.1. PREDICTION OF MARGINAL DENSITY FUNCTIONS AND EXTREME VALUE STATISTICS VIA THE FPK EQUATION

With the external forcing function in equation (9) modelled as broad-band Gaussian white noise excitation with intensity A, such that $f(t) = Aw(t)$, where $w(t)$ has unit intensity, Markov process theory allows transition probability density functions to be obtained via the Fokker–Planck (FPK) equation [26]. Solution of this equation can be used to obtain marginal densities and (approximate) extreme value statistics. In particular the stationary FPK equation associated with equation (9), is written as

$$\frac{1}{2}\sum_{i=1}^{n}\sum_{j=1}^{n} B_{ij}\frac{\partial^2}{\partial z_i\,\partial z_j}[p(\underline{z}) - \sum_{i=1}^{n}\frac{\partial}{\partial z_i}[g_i(\underline{z})p(\underline{z})] = 0 \tag{10}$$

where $n = 2$, $B = 2\pi AA^{\mathrm{T}}$ and $p(\underline{z})$ is the stationary joint probability density function (jpdf) subject to particular boundary (and normalization conditions). Since in general there are no exact solutions of the FPK equation associated with equation (9), use of the finite

TABLE 1

Parameter estimates via the SVF method using simulated data

Target parameter values	Parameter estimates and % errors for reducing simulation step size*					
	$\delta t = 0{\cdot}002$ s		$\delta\tau = 0{\cdot}001$ s		$\delta\tau = 0{\cdot}0005$ s	
	Estimate	% Error	Estimate	% Error	Estimate	% Error
$\alpha_1 = 0{\cdot}812$	1·05	29%	0·892	10%	0·888	9%
$\alpha_2 = 0{\cdot}015$	0·012	−19%	0·014	−8%	0·014	−5%
$\omega_n^2 = 20\,835$	19 771	−5%	20 275	−2%	20 483	−2%
$\gamma\omega_n^2 = 3019$	2061	−32%	2642	−12%	2845	−6%

Duration of sample = 250 s (6875 cycles); large time step $\Delta t = 0{\cdot}002$ s

* Estimates shown are accurate to 3 d.p.; % error calculations use higher precision. The value $A = 200$ is used in the simulation.

element method (see, for example, reference [27]) offers a very accurate and efficient approximation [28]. The unknown nodal values of probability p_i are obtained via the FEM by solving a (sparse) system of $N^n \times N^n$ linear equations (where N is the number of nodes used). The jpdf is integrated to obtain marginal density functions for displacement or velocity variables, and also to obtain approximate extreme value statistics via the mean threshold up crossing rate,

$$v^+(u_T) = \int_0^{+\infty} \dot{z} p(u_T, \dot{z})\, \mathrm{d}\dot{z}, \tag{11}$$

where use of the Poisson assumption [29] allows approximation of the extreme value distribution function,

$$F_M(u_T) = \text{prob}\left\{M(T) \leqslant u_T\right\} = \mathrm{e}^{-v^+(u_T)T}, \tag{12}$$

which is then expressed in terms of the extreme-value exceedance probability:

$$P\left\{M(T) \geqslant u_T\right\} = 1 - F(u_T). \tag{13}$$

TABLE 2

Parameter estimates via the Markov based moment method using simulated data

Target parameter values	Parameter estimates and % errors using different sets of moment equations*					
	second and fourth order		second, fourth and sixth order		second, fourth, sixth and eighth order	
	Estimate	% Error	Estimate	% Error	Estimate	% Error
$\alpha_1 = 0{\cdot}812$	$15{\cdot}6 \times 10^{-6}\ A^2$ 0·624	— −23%	$14{\cdot}0 \times 10^{-6}\ A^2$ 0·56	— −31%	$12{\cdot}8 \times 10^{-6}\ A^2$ 0·512	— −36·9%
$\alpha_2 = 0{\cdot}015$	$0{\cdot}51 \times 10^{-6}\ A^2$ 0·020	— +33%	$0{\cdot}53 \times 10^{-6}\ A^2$ 0·021	— +40%	$0{\cdot}54 \times 10^{-6}\ A^2$ 0·022	— +46·7%
$\omega_n^2 = 20\,835$	13 210	−36·5%	15 524	−25·4%	16 757	19·6%
$\gamma\omega_n^2 = 3019$	4692	+55·4%	3333	+10·4%	2523	16·4%

* Estimates are obtained from an average of 10 different segments of length 250 s (6875 cycles) with $\Delta t = 0.002$ s and $\delta\tau = 0.0005$ s using an intensity value $A = 200$ in the simulations.

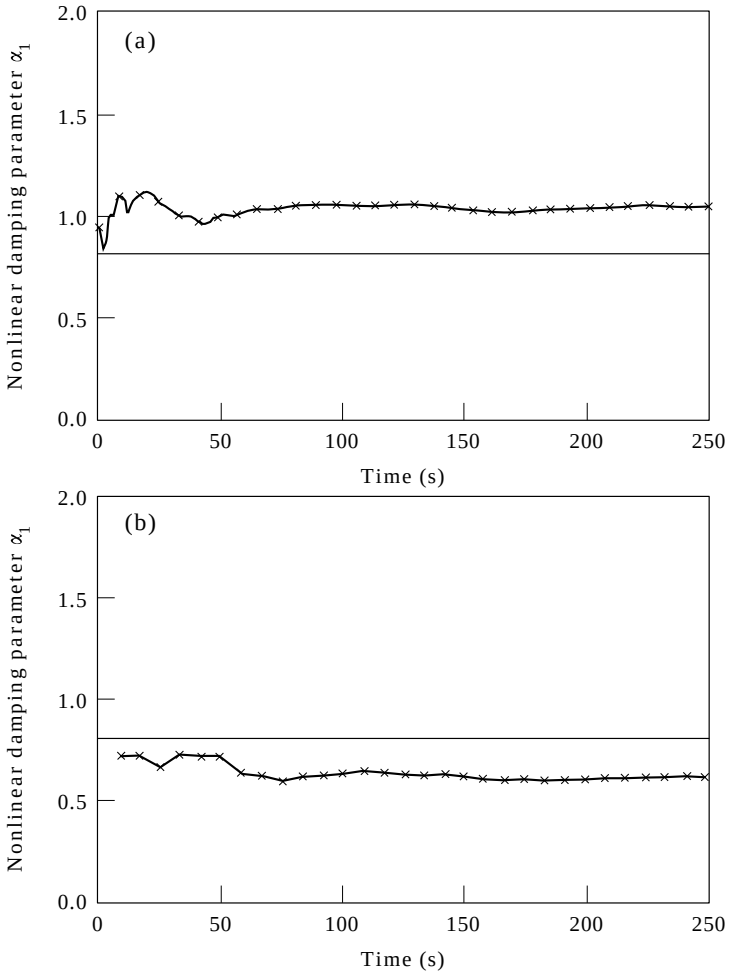

Figure 1. Evolution of nonlinear damping parameter estimate α_1 by using (a) the SVF method, (b) the moment method, for time intervals $\Delta t = 0{\cdot}002$ s and $\delta\tau = 0{\cdot}002$ s (worst case)—the target values are shown as the solid line (——); estimated parameters by $\times$.

Detailed justification of the Poisson assumption and an assessment of the accuracy of this FEM–FPK route to extreme value prediction has been fully examined in reference [28], showing in fact, over a wide probability range, very good agreement with simulation for oscillator models with nonlinear damping. Marginal densities and extreme values will be predicted using this approach in section 5.

3. MATCHED PARAMETER ESTIMATION AND RESPONSE PREDICTION—TESTING WITH SIMULATED DATA

Two parameter estimation techniques are tested here by using noise-free simulated data to assess their suitability in verifying equation (9) when using experimentally generated random data. Simulated data is useful because a good indication of the likely performance and expected accuracy of parameter estimates with real data can be given, without any of the uncertainty associated with the dynamic model. The specific purposes of these tests are (i) to establish the sensitivity of parameter estimates to changes in the sampling rate,

and (ii) to assess the quality of the predicted response statistics obtained when using the dynamic model based on a set of estimated parameters. There are two reasons why knowledge of the required sampling rate is important: first because the experimental data acquisition system (see section 4) may have (as in our case) restricted storage capability (1 Mbyte), such that only relatively short sections of time history can be obtained at high frequency; second, the effect of sensitivity to sampling rate is important in order to assess the impact of small but unwanted phase shifts which occur in simultaneous measurements of force and response. When parameter estimation based on simultaneous measurements of force and response, which require very high frequency sampling, even very small phase differences between measurements will corrupt the parameter estimation process unless full compensation is possible. Satisfactory compensation is difficult to achieve when the measuring instruments themselves behave nonlinearly. The first parameter estimation method tested is the State Variable Filter (see reference [30] for good application of the SVF), and method 2 is based on Markov process theory with the use of stationary moment equations [31]. The SVF requires explicit force and response histories, whereas the moment method requires only response (moments), upon assuming the excitation can be modelled as Gaussian white noise. Implementation details for both methods as given in the Appendix applied to a slightly reduced version of equation (9) by locking parameter $C_1 = 0$ (use of this reduced version for testing these methods is fully justified because the linear damping term, obtained with real data, turns out to be small compared with the non-linear damping terms—see section 5).

Conventional time-domain simulations used in the tests involve three stages: (i) construction of excitation sample paths; (ii) numerical integration (by using Runge–Kutta); and (iii), post-processing for transient removal and collection of stationary responses of length T. In the second stage, a truncated Whitaker filter [32] is used to allow convergence of the numerical integration, because white noise samples of the excitation process are assembled at discrete time intervals of duration Δt, giving a uniformly increasing Nyquist bandwidth $f_n = 1/2\Delta t$ as $\Delta t \to 0$. Normally this has the effect of creating noisier excitation samples as $\Delta t \to 0$. But by fixing Δt, use of the Whitaker filter allows interpolation to smaller time steps $\delta\tau$ generating rapid reduction of the truncation error. Accurate Monte Carlo simulation requires Δt to be suitably chosen to give a Nyquist bandwidth many times

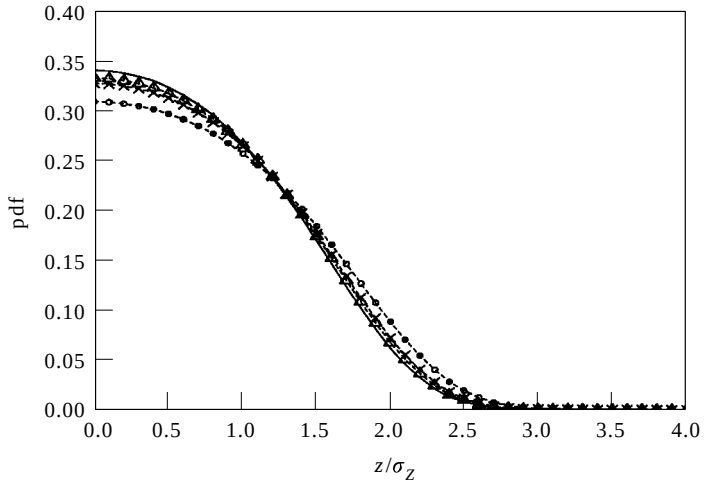

Figure 2. Marginal probability density function for the displacement variable predicted with the FEM by using both target and estimated parameters with different time steps $\delta\tau$ in the SVF method. ——, For target parameters; for estimated parameters: ●, $\delta\tau = 0{\cdot}002$ s; ×, $\delta\tau = 0{\cdot}0015$; △. $\delta\tau = 0{\cdot}0005$ s.

the characteristic bandwidth of the system, with $\delta\tau$ usually selected somewhat smaller to meet the numerical convergence requirements.

In testing both methods, the non-zero target parameter values used for equation (9) are as follows: $\alpha_1 = 0{\cdot}812$, $\alpha_2 = 0{\cdot}015$, $\omega_n^2 = 20835$, $\gamma\omega_n^2 = 3019$, $A = 200$. The target damping and stiffness parameters shown here were actually obtained by using a preliminary study based on the moment method applied to a limited amount of real data taken from the experimental test rig (discussed in section 4—see Figure 6 of section 4). After appropriate integration of accelerometer measurements to obtain displacement time histories, followed by application of the moment method, these particular target parameters were returned. Although this set will ultimately turn out to be different from those obtained using the particular estimation method chosen as a result of the study shortly, it does in fact prove quite adequate for testing against simulated data, the nonlinear parameter estimation capabilities of both methods.

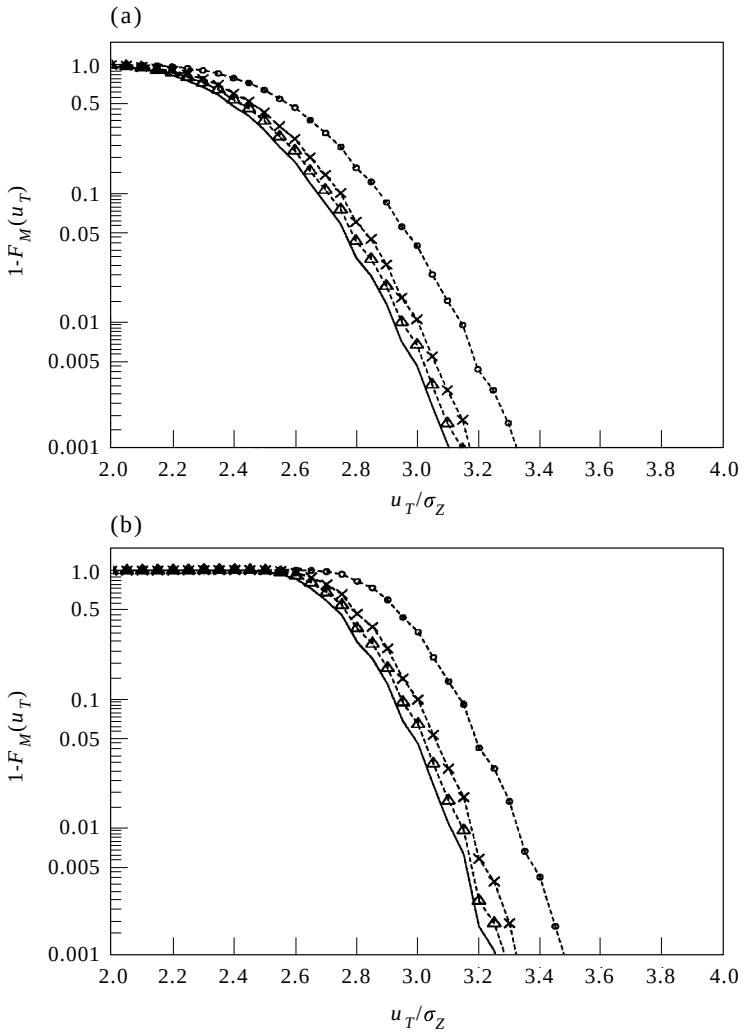

Fig 3. *Caption on opposite page*.

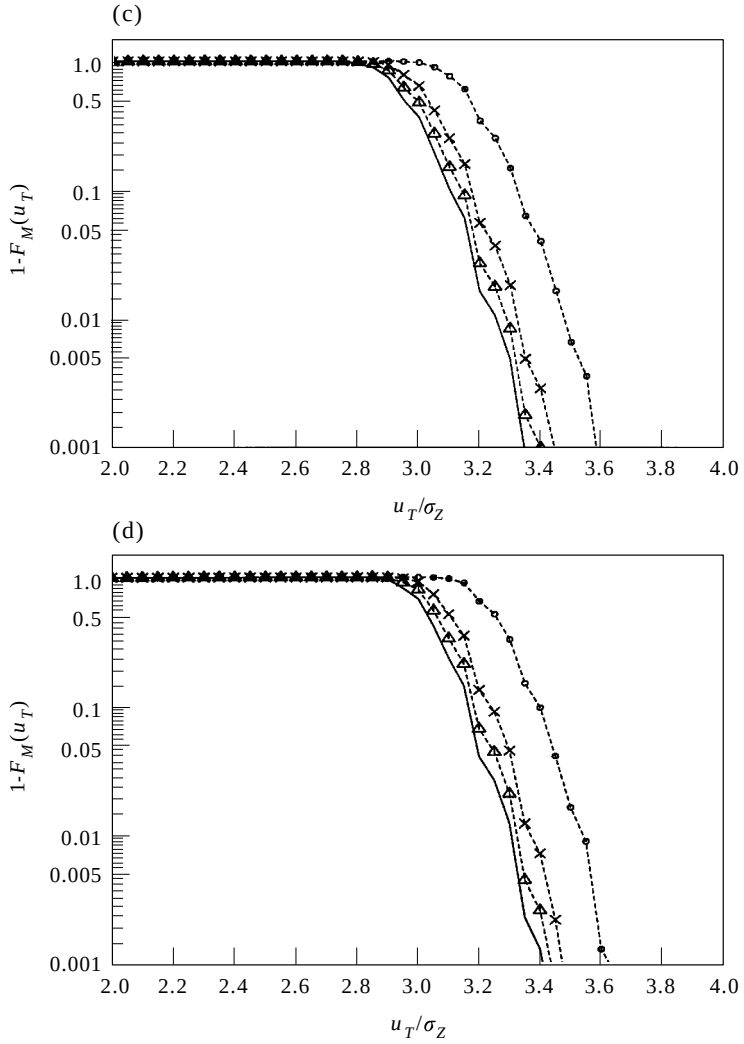

Figure 3. Extreme exceedance probabilities obtained with the FEM using both target and estimated parameters with different time steps $\delta\tau$ in the SVF method (a) $T = 1$ s (27·5 cycles); (b) $T = 10$ s (275 cycles); (c) $T = 100$ s (2750 cycles); (d) $T = 250$ s (6875 cycles). Key as Figure 2.

Band-limited white noise up to a frequency of 250 Hz ($\Delta t = 0{\cdot}002$ s) was used to cover the required response band-width of the model. Simulations of low probability extreme values in reference [28], showed complete convergence at $\delta\tau = 0{\cdot}001$ s for a similar system with similar parameters. Presentation of the results for two sets of tests are shown in two parts: first we show the effect on the SVF of varying the sampling rate from 500 Hz to 2000 Hz; and second we show the effect of using different sets of equations in the moment method (see the Appendix), and report on the findings of similar sampling rate sensitivity tests for the moment method.

In the SVF method tests, excitation and corresponding response histories of 250 s duration (6875 cycles) are generated by simulation. Since the simulation method generates only discrete samples, intermediate points are needed—these are also obtained by using interpolation via the Whitaker filter allowing the small time step $\delta\tau$ in the fourth order

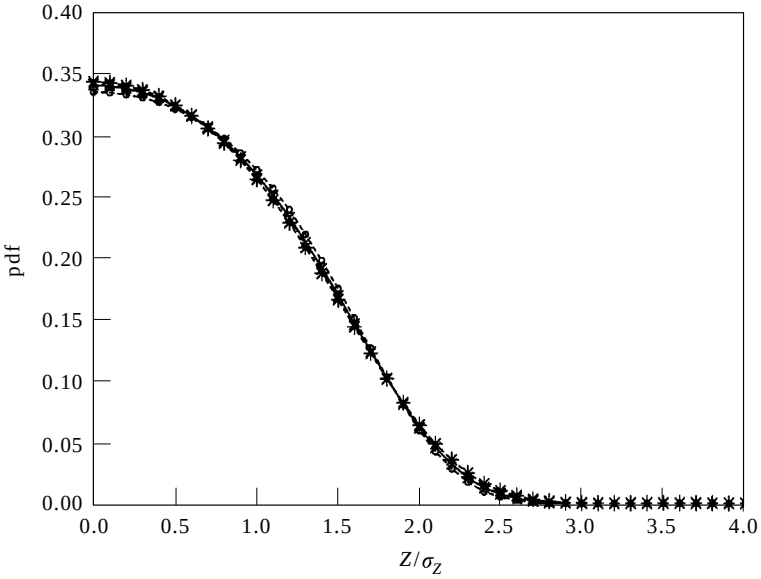

Figure 4. Marginal probability density function for the displacement variable, predicted with the FEM by using both target and estimated parameters via different sets of equations in the moment method. ——, Exact parameters; estimated parameters: ○, (2, 4); × (2, 4, 6); ∗, (2, 4, 6, 8).

numerical integration scheme to be reduced from 0·002 s to 0·0005 s, with the results shown in Table 1.

The test shows only the SVF estimator converging since the simulations have converged for non-extreme values at $\delta\tau = 0{\cdot}002$ s—there is in fact still some change in the estimates between 0·001 s and 0·0005 s suggesting the SVF estimation method has not yet converged at 0·001 s. The results shown in Table 1 would indicate that the SVF will give acceptably small nonlinear parameter estimation errors provided $\delta\tau$ is not greater than 0·001 s (i.e. a sampling rate >1000 Hz must be used).

In testing the moment method, different sets of moment equations were initially used (see the Appendix). Here three sets are applied to simulated response data of 250 s duration with a time step of $\delta\tau = 0{\cdot}0005$ s. These three tests involve application of: the second and fourth moment equations, the second, fourth, and sixth, and the second, fourth, sixth and eight equations. Although the method requires only response histories, the statistical scatter in the final parameter estimates when using single 250 s simulated data sections is very much higher than with the SVF method. To reduce this scatter, parameter estimates obtained from 10 different sections are averaged to obtain mean estimates. These mean values are shown in Table 2.

Although the moment method [31] outlined in the Appendix gives estimates of damping-to-intensity ratio (not explicit values), a target excitation intensity $A = 200$ is used to assess the level of accuracy in explicit values. Different sampling frequencies were also examined in the same way as for the previous SVF test, namely by using three values $\delta\tau = 0{\cdot}002$, $\delta\tau = 0{\cdot}001$, and $\delta\tau = 0{\cdot}0005$ s respectively, but there was no observable difference between the corresponding parameter estimates (confirming convergence of the simulations).

To give an indication of the rate of convergence obtained when using both methods (at the worst but in fact necessary sampling rate) Figure 1(a) and 1(b) show the convergence of the estimate for the nonlinear damping parameter α_1—demonstrating that roughly

similar convergence rates are obtained and confirming that most of the data is needed. It must be stressed however that the SVF estimate would of course be significantly more accurate when using faster sampling rates.

Although the performance of both the SVF and moment methods can be judged to some extent from Tables 1 and 2, results can be rather misleading since the accuracy of the estimated parameters must be measured in terms of the different response statistics for which they will ultimately be used. A better test therefore requires direct comparison between response statistics based on the model when using target parameters, compared with those obtained when using estimated parameters. For this purpose statistics based on a finite element solution of the FPK equation are appropriate since they are largely free from the statistical variability inherent in the simulations. Here the response amplitude marginal probability density function and the extreme value exceedance probability (for fixed duration of length T) are predicted via the route described in section 2.1. The finite element method used is a 31×31 mesh over a quarter region—this is quite adequate for

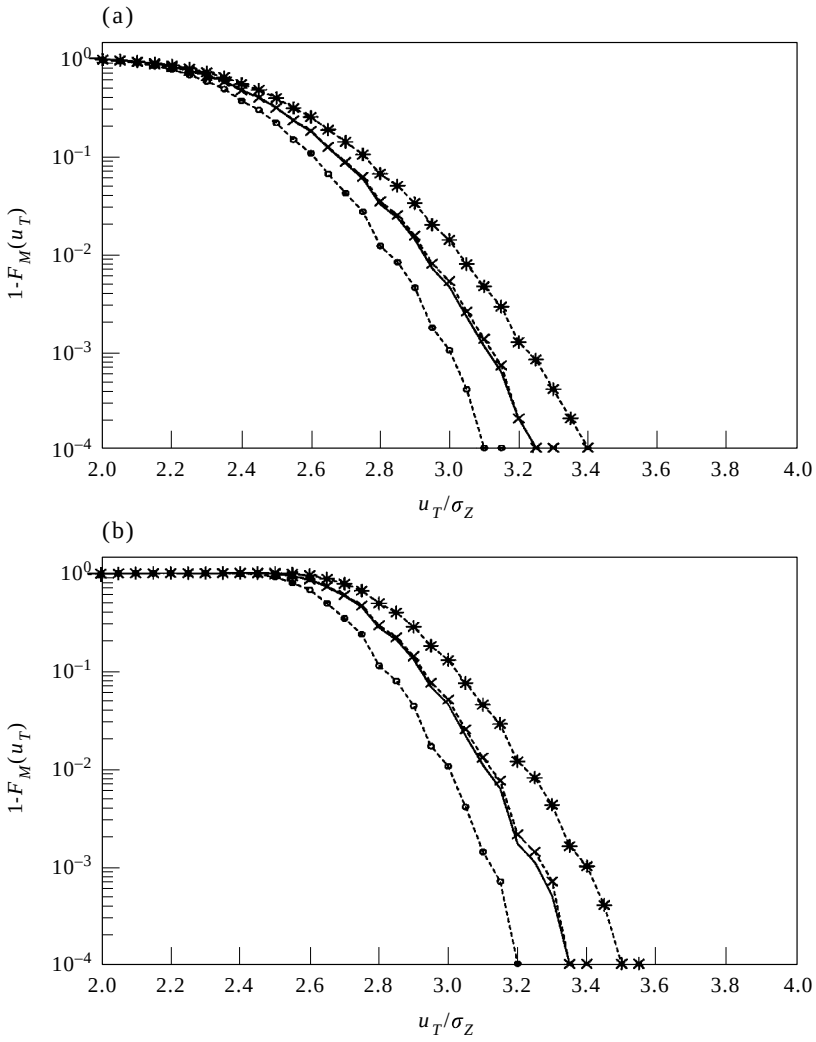

Figs 5a–b. *Caption overleaf*

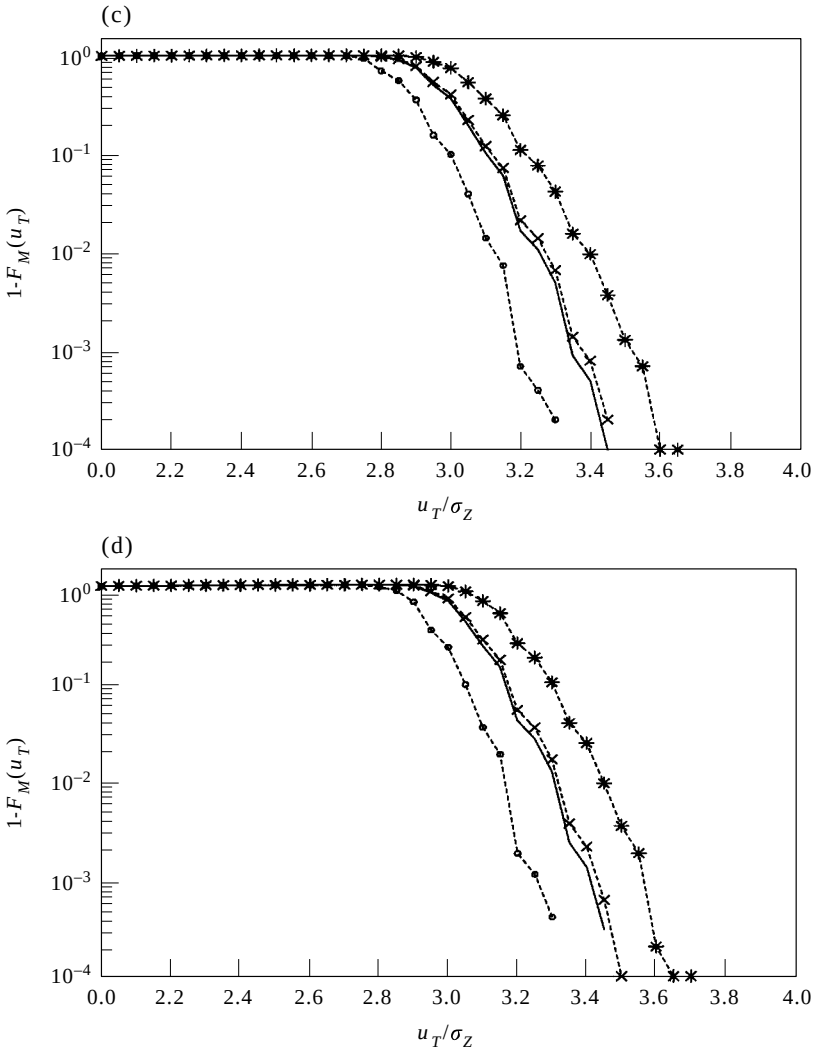

Figure 5. Extreme exceedance probabilities predicted with the FEM by using both target and estimated parameters and different sets of equations in the moment method: (a) $T = 1$ s (27·5 cycles); (b) $T = 10$ s (275 cycles); (c) $T = 100$ s (2750 cycles); (d) $T = 250$ s (6875 cycles). Key as Figure 4.

extreme response prediction [28]. To predict the joint probability density function and the extreme response for different durations when using parameter estimates obtained with the SVF method described in the Appendix, the theoretical intensity $A = 200$ is used, without attempting to estimate it from the excitation process.

The response marginal density function based on the exact parameters and the FEM–FPK solution method is compared in Figure 2 with the corresponding density obtained with the SVF estimates. It can be seen that for progressively smaller time step, the predicted marginal density improves approaching the target density function. Figure 3(a–d) show a comparison of extreme values exceedance probabilities down to 10^{-3} for durations of $T = 1$, 10, 100, and 250 s respectively (i.e. 27·5, 275, 2750 and 6875 cycles). Confident extreme value exceedance probabilities down to 10^{-2} (when using simulated or

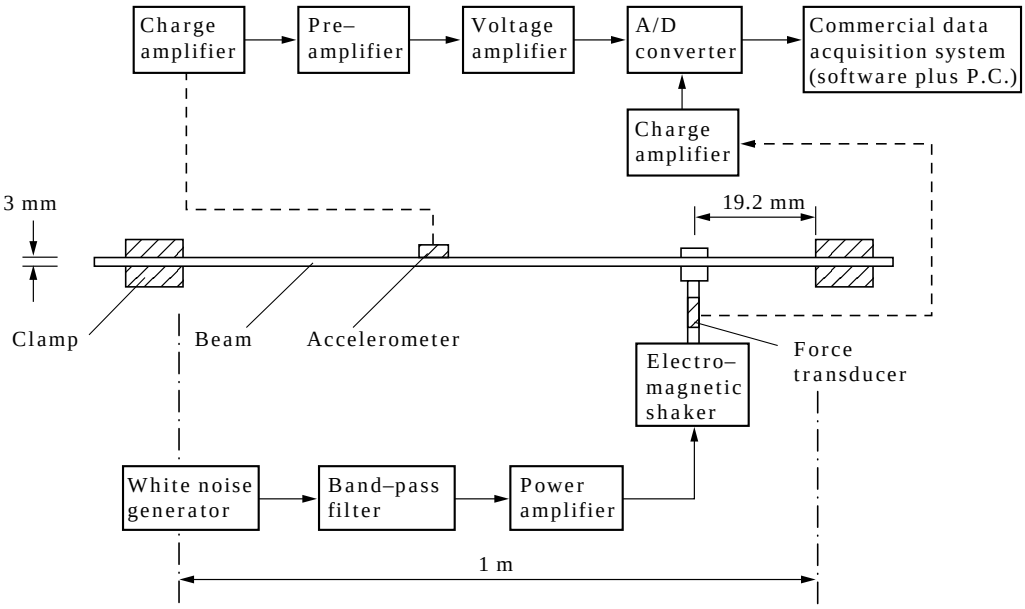

Figure 6. Experimental rig in diagrammatic form showing plan view of the clamped-clamped beam with effective dimensions 1 m × 25 mm × 3 mm.

experimental data) require, for each duration of length T, about 1000 samples of $M(t)$ [used in equation (13)]. This places very heavy demands on data requirements.

To turn now to the moment method, Figure 4 shows probability density functions predicted with the FEM-FPK approach when using target parameters, compared with use of estimated parameters via different combinations of moment equations. Figure 5(a–d)

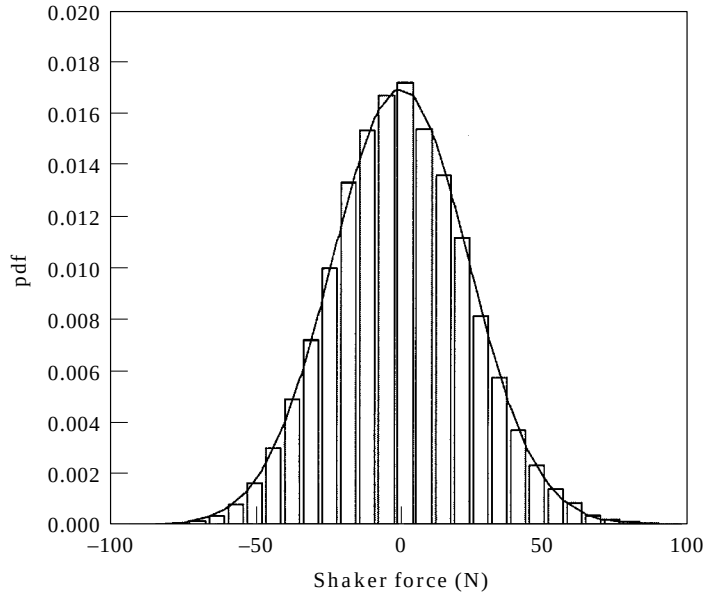

Figure 7. Probability density estimate from sample of measured shaker force compared with normal density with same mean and standard deviation.

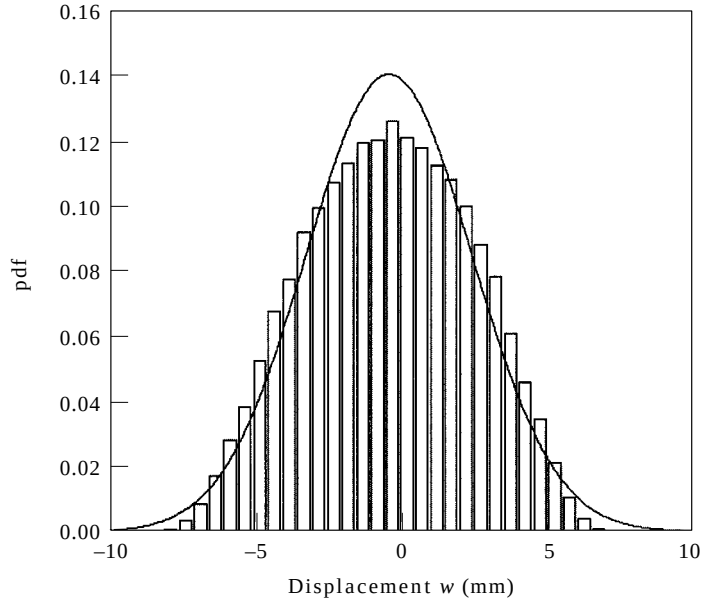

Figure 8. Probability density estimate from sample of the measured central beam deflection compared with normal density with same mean and standard deviation.

shows corresponding extreme value exceedance probabilities down to 10^{-4} for durations of $T = 1$ (27·5 cycles), 10 (275 cycles), 100 (2750 cycles) and 250 (6875 cycles) seconds respectively. In each figure, the extreme response statistics are based on the target parameters compared with those obtained from (i) the set of second and fourth, (ii) the second, fourth and fifth, and (iii) the second, fourth, sixth and eight moment equations. Although the individual parameters returned by the moment method are not very accurate, treated as a single set in the equation of motion, these estimates are very good for predicting both marginal densities and extreme response statistics via the FPK–FEM approach—this would suggest a degree of matching between the Markov based parameter estimation method and the Markov based predictions (i.e. by using the FPK equation).

Three relevant conclusions can be reached from these tests in respect of their suitability for use on real experimental data:

(1) The SVF method is very sensitive to sampling rate, therefore in some applications this may create data storage problems or difficulties with phase shift in real measurements.
(2) The moment method cannot be judged on the specific parameter estimates alone, but rather in terms of predicted response statistics.
(3) The particular set of moment equations used for parameter estimation is important subsequently for prediction of extreme response statistics.

Since there were indeed both storage limitations in our experimental data acquisition system, and problems of phase shift between simultaneous measurements of force and response, these findings justified in our application use of the moment method rather than SVF based parameter estimation. It must again be stressed however that under different circumstances, the findings of Table 1 show that the SVF method would of course be more appropriate.

4. EXPERIMENTAL BEAM RIG AND MEASUREMENT DETAILS

The experimental test rig is shown schematically in plan view in Figure 6. The beam was selected for its appropriate dynamic characteristics to allow large amplitude vibration and extreme value data collection (at a suitable sampling rate) from hundreds of thousands of high amplitude vibration cycles without change in mechanical properties [33]. To achieve the required dynamic characteristics, upper and lower limits were imposed on the lowest resonance frequency. The beam dimensions were therefore chosen so that, with appropriate band-limited excitation, only the lowest (nonlinear) resonance frequency would be excited and that response amplitudes would exhibit the sort of nonlinear behaviour typically occurring on highly loaded structures. To meet these demands a steel beam was used of length $L = 1000$ mm, depth $d = 3$ mm and breadth $b = 25$ mm with $E = 190 \times 10^9$ N/m^2 and density $\rho = 7580$ kg/m^3, giving the first three small amplitude linear vibration frequencies of 15 Hz, 42 Hz and 82 Hz respectively.

A standard electromagnetic shaker, capable of producing a maximum force of 100 N with correct bandwidth, was used to excite the beam. This was connected directly near one end of the beam (19·2 mm from one of the clamps) via a force transducer to allow moderate displacement of the shaker head but to minimize the impact of the shaker dynamics. The shaker gave a maximum peak-to-peak displacement of 16 mm over a frequency range 1·5 Hz–9 kHz. Excitation signals were generated by using function and noise generators via a variable filter allowing fine tuning of the white noise bandwidth. To construct

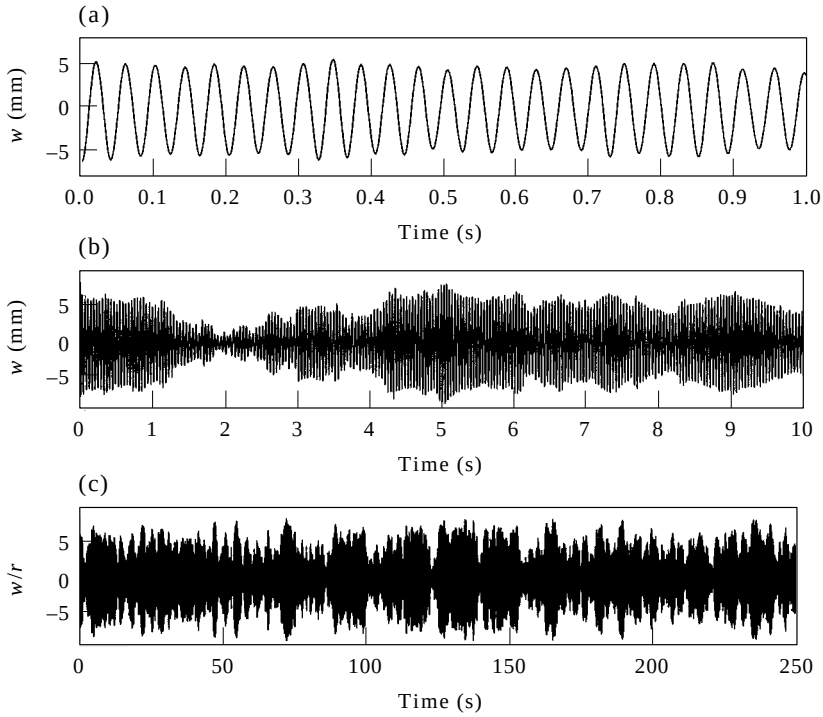

Figure 9. Typical measured time history for the central beam displacement (absolute and normalized. (a) 25 cycles; (b) $\sim$ 250 cycles; (c) normalized displacement ratio w/r for $\sim$6250 cycles.

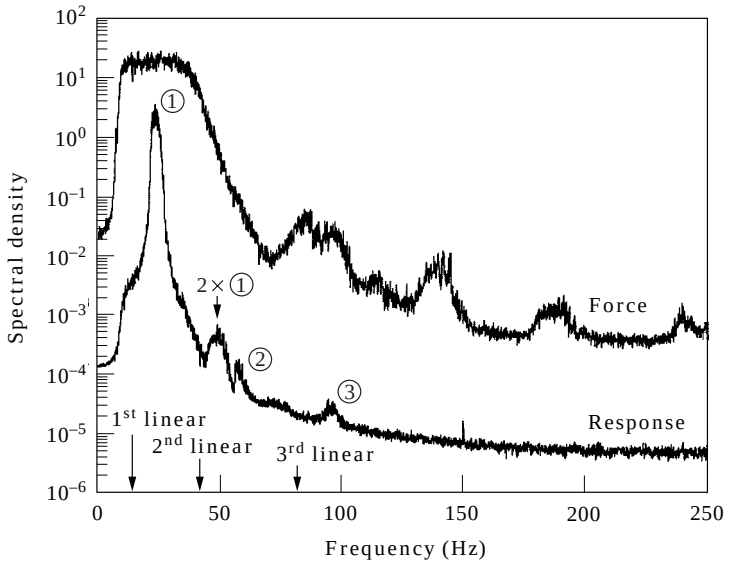

Figure 10. Power spectral density estimates from the measured force and central beam displacement showing the locations of the first three linear undamped natural frequencies.

band-limited white noise excitation signals with sufficient power, the signal generator outputs were fed via high pass and low pass filters (with cut-off frequencies set at 10 Hz and 40 Hz respectively) and finally into a power amplifier. Force measurement was obtained by using a (Kistler type 9031) transducer capable of being used for both static and dynamic applications.

A single accelerometer (Bruel & Kjaer type 4332) was located at the beam mid-span position. To obtain integrated displacements above a frequency of 10 Hz, sampled acceleration signals at 500 Hz were fed into a very high input impedance charge amplifier (vibration pick-up preamplifier type 2625). These displacement signals were fed into a null-adjuster voltage amplifier which also removed d.c. offset introduced by the integration network. Calibration of the accelerometer used a capacitive type displacement transducer (Wayne Kerr) giving a working range of 0–8 mm, and accuracy of 1% with linearity better than 2%. This was not used for large amplitude beam vibration owing to its limited working range, typically being a little less than measured extreme values. The capacitive transducer itself was calibrated dynamically (by using a moving table) and was then used to calibrate measured displacements obtained from the accelerometer (positioned on the shaker head driven by a 20 Hz signal).

For parameter estimation, force and displacement data could only just be captured without storage problems with our commercial system in single records of 250 s duration at 0·002 s. For direct extreme value measurement however, the largest maximum was required for each duration of length T, with tests necessarily repeated several hundred times to enable sufficient global maxima to be captured for each duration. This placed very heavy demands on storage so the capture procedure had to be very selective by storing only the maximum values, not the entire record. To ensure no change in the mechanical properties of the beam over these very long experiments, 250 s long sections were periodically captured specifically to confirm repeatable results. For both types of data collection a sampling rate of 500 Hz was used.

5. MODEL VERIFICATION USING MEASURED DATA AND MOMENT BASED PARAMETER ESTIMATION

The Markov based model verification and prediction approach developed in section 3 is now applied to data generated with the purpose-built experimental rig. In total, ten semi-empirical sub-models obtained from equation (9) are examined—these are conveniently labelled A–H as follows:

$$(A) \quad \ddot{z} + C_1\dot{z} + \omega_n^2 z = Aw(t); \tag{14}$$

$$(B) \quad \ddot{z} + C_1\dot{z} + \omega_n^2(1 + \gamma z^2)z = Aw(t); \tag{15}$$

$$(C) \quad \ddot{z} + \alpha_1\dot{z}z^2 + \omega_n^2(1 + \gamma z^2)z = Aw(t); \tag{16}$$

$$(D) \quad \ddot{z} + C_1\dot{z} + \alpha_1\dot{z}z^2 + \omega_n^2(1 + \gamma z^2)z = Aw(t); \tag{17}$$

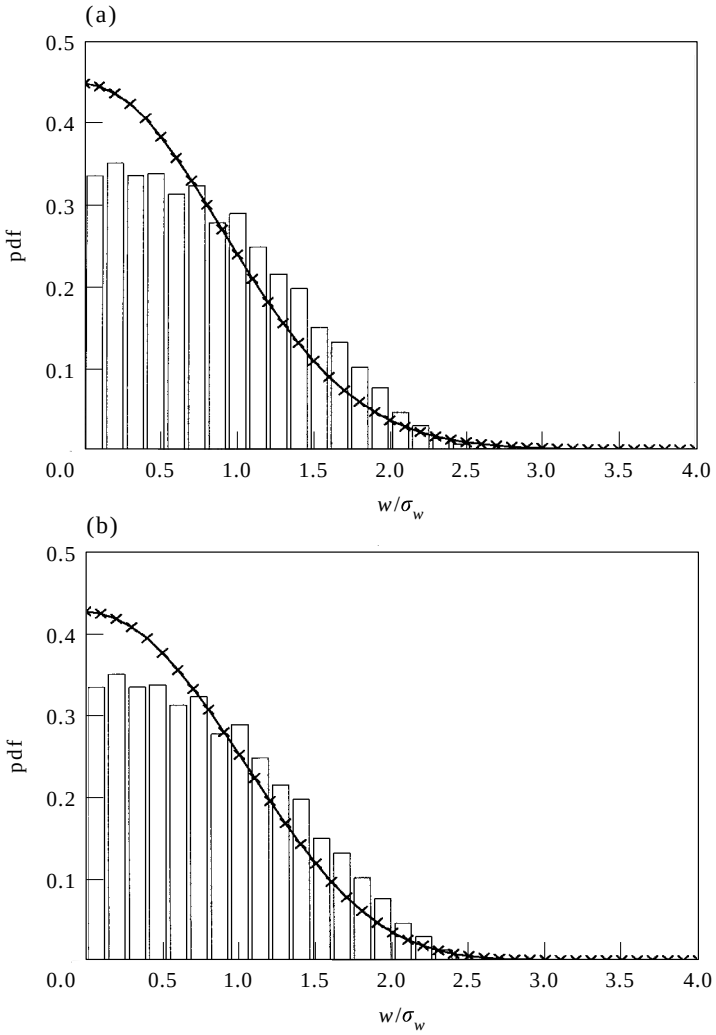

Figs 11a–b. *Caption on page 22.*

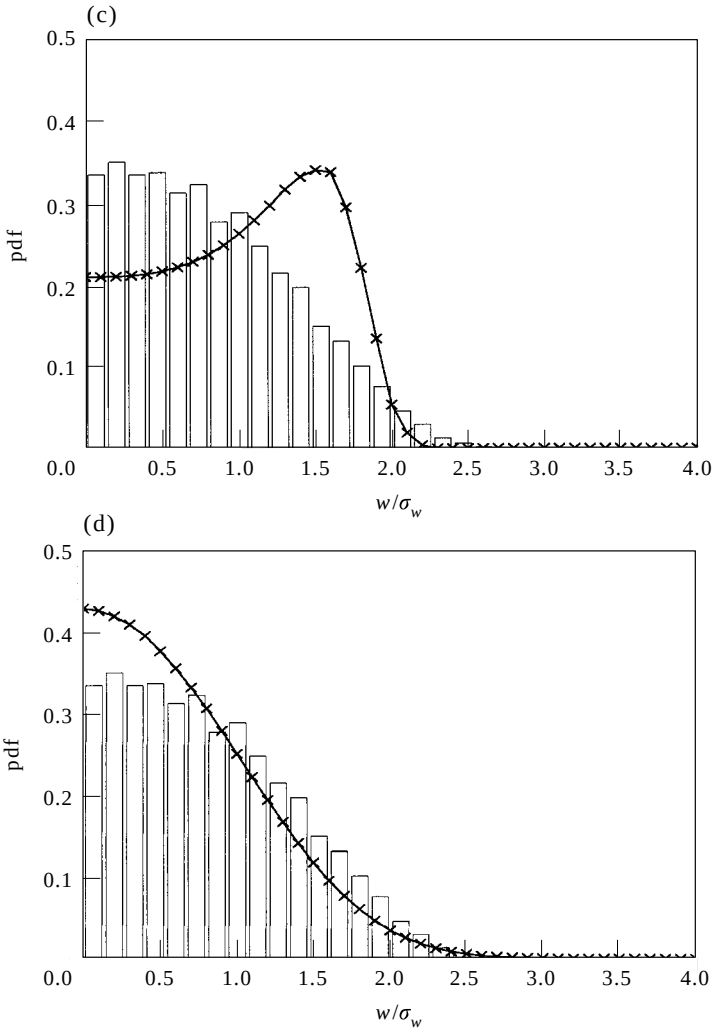

Figs 11c–d. *Caption on page* 364

$$(E) \quad \ddot{z} + \alpha_2 \dot{z}|\dot{z}| + \omega_n^2(1 + \gamma z^2)z = Aw(t); \tag{18}$$

$$(F) \quad \ddot{z} + C_1\dot{z} + \alpha_2 \dot{z}|\dot{z}| + \omega_n^2(1 + \gamma z^2)z = Aw(t); \tag{19}$$

$$(G) \quad \ddot{z} + \alpha_1 \dot{z}z^2 + \alpha_2 \dot{z}|\dot{z}| + \omega_n^2(1 + \gamma z^2)z = Aw(t); \tag{20}$$

$$(H) \quad \ddot{z} + C_1\dot{z} + \alpha_1 \dot{z}z^2 + \alpha_2 \dot{z}|\dot{z}| + \omega_n^2(1 + \gamma z^2)z = Aw(t). \tag{21}$$

Models A–G are obtained by locking to zero specific parameters in model H [namely the semi-empirical SDOF model equation (9)]. The suitability of each model is assessed in terms of its performance at marginal probability density level, and then the best model is examined in terms of extreme value exceedance probabilities over different durations. To minimize the statistical variability in the parameter estimates obtained using an appropriate set of second, fourth, and sixth order moment equations (as tested in section 3), a total of 10 parameter estimation sets are averaged for each model. The measured displacement marginal density functions are compared with prediction based on the mean

parameter estimates using finite element solutions of the FPK equation outlined in section 2. Likewise, for the best model, extreme value exceedances are compared with predictions (also see section 2) in the probability range 10^{-3}–10^{-4} for durations $T = 1$, 10, 20 and 40 s.

The moment based parameter estimation method, tested on simulated data in section 3, model G was used rather than model H (see the Appendix). This was justified because the impact of the linear damping contribution was assumed to be very much smaller than the non-linear damping. To confirm this assumption, the full set of second, fourth, and sixth order moment equations for model H (derived in the same way as shown in the Appendix) were used here on the real data. These equations are given explicitly as follows.

Moment equations for model H. The stiffness parameters are estimated from the respective set of moment equations (22)–(27) by using the second order equation

$$k_2[\omega_n^2 E(z_1^2) + \gamma\omega_n^2 E(z_1^4)] = k_1 E(z_2^2), \tag{22}$$

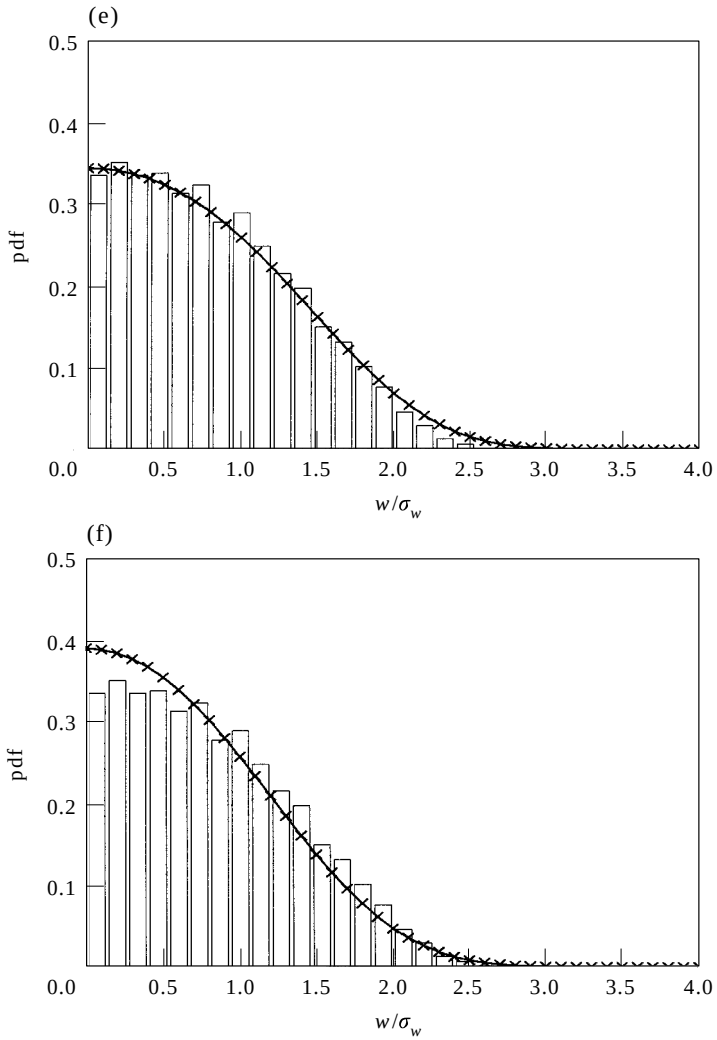

Figs 11e–f. *Caption overleaf*

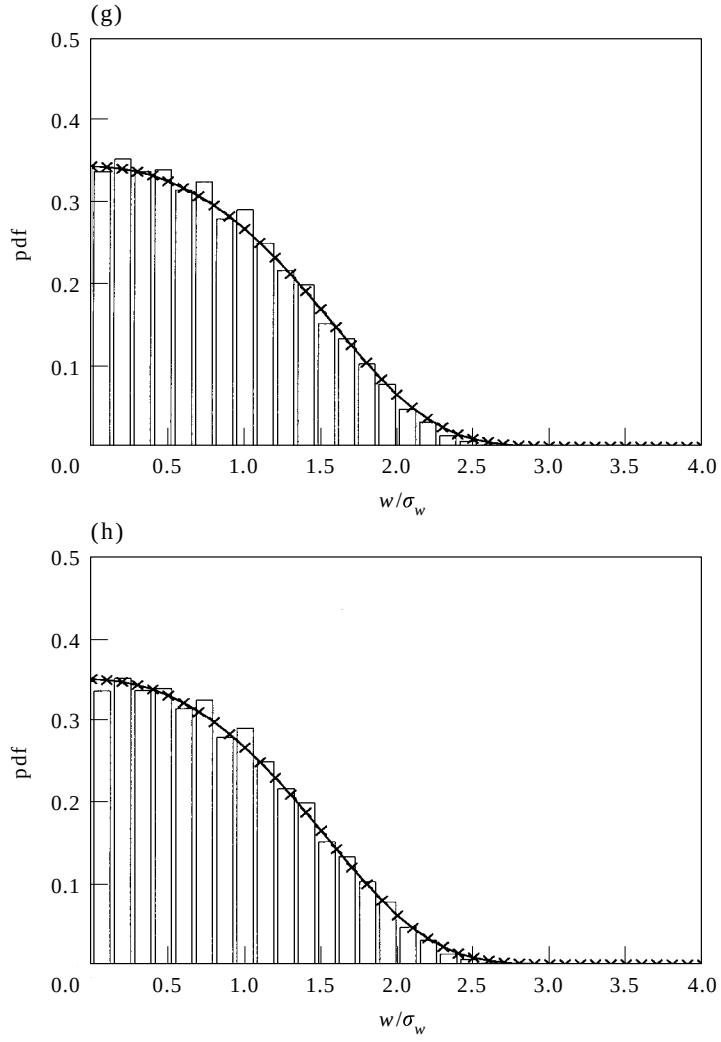

Figs 11g–h.

Figure 11. Measured probability density function for the central beam displacement compared with prediction via the FEM by using the mean parameter estimates from the moment method: (a)–(h) correspond to models A–H respectively. □, measured pdf; ×, predicted pdf.

the fourth order equations

$$k_2[\omega_n^2 E(z_1^2 z_2^2) + \gamma\omega_n^2 E(z_1^4 z_2^2)] = k_1 E(z_2^4), \tag{23}$$

$$k_2[\omega_n^2 E(z_1^4) + \gamma\omega_n^2 E(z_1^6)] = k_1 E(z_1^2 z_2^2), \tag{24}$$

and the set of sixth order equations

$$k_2[\omega_n^2 E(z_1^2 z_2^4) + \gamma\omega_n^2 E(z_1^4 z_2^4)] = \pi A^2 k_2(k_2 - 1)E(z_1 z_2^3) + k_1 E(z_2^6), \tag{25}$$

$$k_2[\omega_n^2 E(z_1^4 z_2^2) + \gamma\omega_n^2 E(z_1^6 z_2^2)] = k_1 E(z_1^2 z_2^4), \tag{26}$$

$$k_2[\omega_n^2 E(z_1^6) + \gamma\omega_n^2 E(z_1^8)] = k_1 E(z_1^4 z_2^2), \tag{27}$$

and both linear and non-linear damping parameters are estimated from the sets of equations (28)–(33) by using the second order equation

$$k_2[C_1E(z_2^2) + \alpha_1E(z_1^2z_2^2) + \alpha_2E(z_2^2|z_2|)] = \pi A^2k_2(k_2 - 1), \tag{28}$$

and fourth order equations

$$k_2[C_1E(z_2^4) + \alpha_1E(z_2^4) + \alpha_2E(z_2^4|z_2|)] = \pi A^2k_2(k_2 - 1)E(z_2^2) \tag{29}$$

$$k_2[C_1E(z_1^2z_2^2) + \alpha_1E(z_1^4z_2^2) + \alpha_2E(z_1^2z_2^2|z_2|)] = \pi A^2k_2(k_2 - 1)E(z_1^2), \tag{30}$$

and the sixth order equations

$$k_2[C_1E(z_2^6) + \alpha_1E(z_1^2z_2^6) + \alpha_2E(z_2^6|z_2|)] = \pi A^2k_2(k_2 - 1)E(z_2^4) \tag{31}$$

$$k_2[C_1E(z_1^2z_2^4) + \alpha_1E(z_1^4z_2^4) + \alpha_2E(z_1^2z_2^4|z_2|)] = \pi A^2k_2(k_2 - 1)E(z_1^2z_2^2), \tag{32}$$

$$k_2[C_1E(z_1^4z_2^6) + \alpha_1E(z_1^6z_2^2) + \alpha_2E(z_1^4z_2^2|z_2|)] = \pi A^2k_2(k_2 - 1)E(z_1^4). \tag{33}$$

Here $E(\cdot)$ is the expectation operator and is applied to the time histories in the form of a sample averaging operator, and in each equation $k_1 + k_2 =$ the equation order, and k_1 is indexed from $k_1 = 0, 1, \ldots$.

Figure 7 shows a typical measured excitation force probability density function compared with a target Gaussian density with the same mean and standard deviation. Figure 8 shows a typical probability density estimate for the central beam displacement also compared with a target Gaussian density with the same moments. Time histories for the measured central beam displacement are shown in Figure 9: i.e. in absolute terms for Figure 9(a) and 9(b) corresponding to 25 cycles and 250 cycles respectively, and in terms of normalized displacements in Figure 9(c) showing a full record of 250 s (6250 cycles). Figure 10 shows a typical measured force power spectral density and a typical PSD for the central beam displacement. The first, second and third non-linear resonances are identified on the figure as ① ② and ③ respectively along with the small amplitude linear undamped free vibration frequencies. A peak response frequency at double the first nonlinear resonance frequency is also identified on Figure 10 and marked as $2 \times$ ①. An

TABLE 3

Averaged parameter estimates obtained with the Markov moment method

	Magnitude of parameter mean values and the corresponding 95% confidence limits *(sample size $n = 10$)									
	Damping						Stiffness			
	$(C_1/A^2) \times 10^{-6}$		$(\alpha_1/A^2) \times 10^{-6}$		$(\alpha_2/A^2) \times 10^{-6}$		ω_n^2		$\gamma\omega_n^2$	
Model	Mean	95% C.L.	Mean	95% C.L.	Mean	95% C.L.	Mean	95% C.L.	Mean	95% C.L.
A	177.6	±12.5	—	—	—	—	22 276	±360	—	—
B	177.6	±12.5	—	—	—	—	15 573	±493	2322	±249
C	—	—	242.8	±34.4	—	—	17 573	±493	2322	±249
D	179.6	±13.4	−2·7	±2.0	—	—	17 573	±493	2322	±249
E	—	—	—	—	0.54	±0.07	17 573	±493	2322	±249
F	100.3	±22.6	—	—	0.24	±0.11	17 573	±493	2322	±249
G	—	—	19.5	±2.9	0.50	±0.07	17 573	±493	2322	±249
H	13.5	±56.6	18.2	±7.9	0.47	±0.20	17 573	±493	2322	±249

* Individual estimates for each sample obtained with the set of second, fourth and sixth order moment equations. 95% confidence limits are obtained using the t distribution with 9 degrees-of-freedom, giving confidence limits = 2·26 × standard error in the mean (defined as the individual sample standard deviation/$\sqrt{n}$).

example of a typical estimate of the measured displacement mean and standard deviation is $-0{\cdot}44$ mm and $2{\cdot}85$ mm respectively giving a normalized displacement for this beam $(w/r)_{rms} = 3{\cdot}3$ and largest normalized extreme value $w_{\max}/r \approx 10$—therefore this beam vibration is highly nonlinear. The performance and suitability of the different dynamic models A–H is assessed by direct comparison of the predicted marginal density obtained via the FPK equation with an histogram estimate of the measured marginal density function. Figure 11(a)–(h) shows these comparisons for models A–H. Table 3 shows averaged parameter estimates obtained from 10 sets of measured data using the moment method. The individual sets of parameter estimates obtained for each of the 10 samples is for reasons of space not shown. However in addition to estimated mean values, 95% confidence limits in the mean value estimates are shown, based on a sample size $n = 10$, with implicit assumption of normally distributed parameter estimates. Application of the method of equivalent linearization to the average damping obtained for model H gives a value of $1{\cdot}38\%$ critical—which for this particular set of samples, implies that most of the

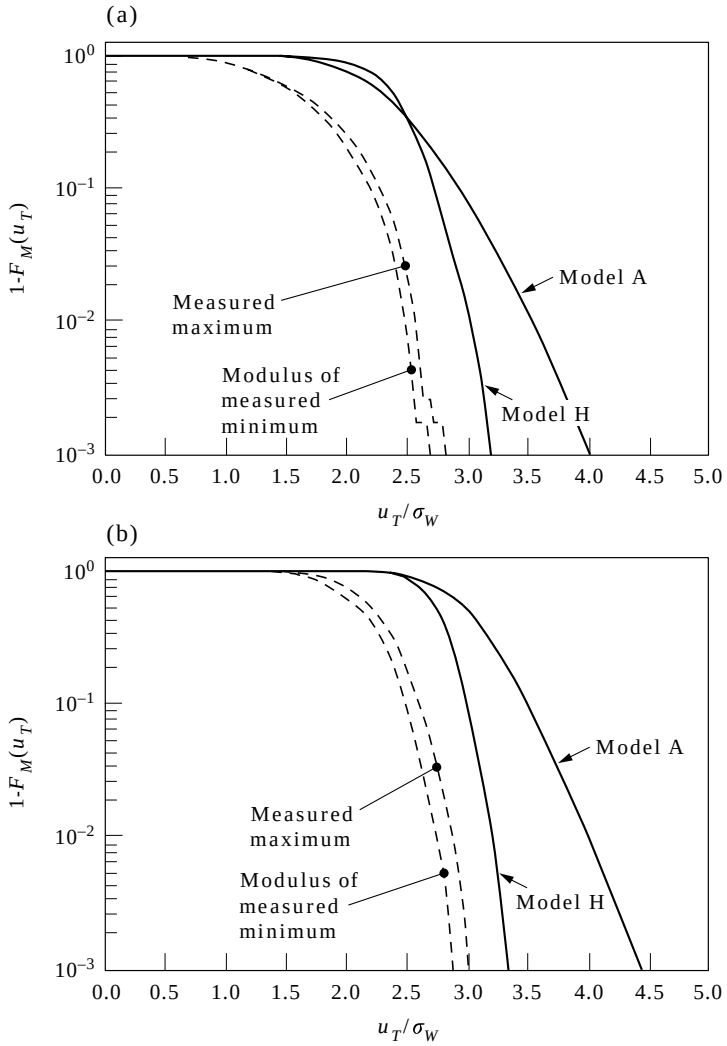

Figs 12a–b *Caption opposite*.

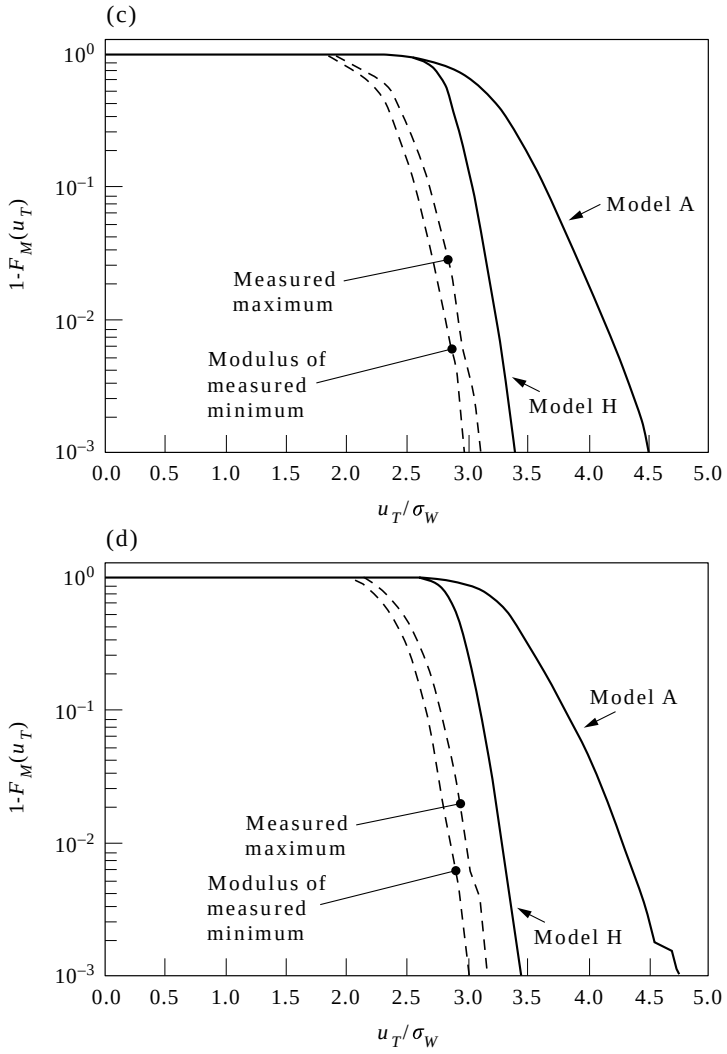

Figure 12. Measured extreme value exceedance probability for the central beam displacement compared with prediction via the FEM by using the mean parameter estimates from the moment method for the best fit (model H), and the worst (model A, linear). (a) $T = 1$ s; (b) $T = 10$ s, (c) $T = 20$ s; (d) $T = 40$ s.

damping is derived from the nonlinear part since the contribution from the average C_1 estimate alone, represents only about 0·18% critical. This adds justification to the assumption made in section 3 regarding parameter C_1 being small, even though the confidence in the damping parameters for model H is lower than for model G, a point discussed further shortly.

By contrast, extreme value exceedance probabilities were predicted for the linear models A–H, as obtained by using the method described in section 2, and compared with experimental measurements corresponding to four different durations $T = 1$, 10, 20, and 40 s respectively. These predictions are based on the same set of parameters used to predict the marginal densities as shown in Figure 12(a–d) down to probability levels of 10^{-3}, where predictions for models A and H are selected to show the best and worst cases, based on their respective performances at the marginal density level. Extreme value predictions for

models B–G (not shown) are bounded between predictions shown for models A and H. Measured extreme value exceedance probabilities for (positive) global maxima, and for absolute values of global minima, are shown to indicate any vibration asymmetry. Note that measurement of extreme exceedances down to these sort of probability levels takes considerable time. For example, in our experiments, collection of a total of 1150 extreme values needed for a duration $T = 40$ s, took more than 20 h of real time continuous measurement.

5.1. DISCUSSION OF RESULTS

First a comment is in order about the strength of nonlinearity evident in the measured vibration: Figure 10, showing the comparison of the force and response power spectral densities, indicates the relative shift in position of the resonance peaks compared with the linear undamped natural frequencies and confirms that these beam vibrations are indeed highly nonlinear. Note that the relative magnitude of the second resonance peak ②, is as expected many orders of magnitude smaller than the first nonlinear resonance peak ① since the displacements correspond to a mid-span measurement—effectively at a node where the second mode responses should theoretically be zero. This information is obviously insufficient to confirm that the second resonance amplitude, resulting from the upper frequency tail of the band-limited white noise excitation, is insignificant. This was confirmed by measurement away from the mid-span position. Note that the peak at a frequency twice the first resonance (indicated by $2 \times$ ①) confirms some small degree of vibration asymmetry probably caused by the shaker or non-isotropic material properties.

Next, the results shown in Table 3, demonstrate how the damping model seems to be very sensitive to forcibly locking individual terms to zero. This is particularly evident in the change from model C to model D. However by the time the full model H is used, the relative magnitude of the linear damping term seems to have diminished considerably. Note the 95% confidence limits shown in Table 3 give an indication of the statistical scatter in the average parameter values and therefore an indication of the parameter estimation errors one would expect from the effects of statistical variations in the data alone. In assessing the implications of this scatter, a clear distinction has to be made between the stability of the model calibration process when using the moment method, and the quality of the model itself—this distinction being focused mainly on models G and H. It can be seen from the confidence limits constructed for model G in Table 3, when compared with the (second, fourth and sixth order) % error column of Table 2 (which applies to model G only, for which the linear parameter is locked to zero) that statistical fluctuation in the moment method is significantly smaller than the errors obtained via the simulation study. Therefore, from a statistical viewpoint, high confidence can be attached to the mean damping parameters obtained for model G, whose calibration can be regarded as very stable. By contrast, the lower level of confidence indicated for calibration of model H, would imply (from a statistical viewpoint) that a larger variation in mean parameters is possible, including a significant linear term. This suggests that calibration of model H is very much less stable than model G. But an important finding of the simulation study in section 3 was that errors in the moment based parameter estimates should not be looked at in isolation from the predicted probabilities when using the FPK equation, which are not sensitive to these individual errors owing to correlation between the parameter estimates (and a convergence study shows that for increasing sample size n, the predicted probability density funtions, based on parameter estimates for models A–H, converge for practical purposes, by the time $n = 10$). Furthermore Figure 11(g) and 11(h) clearly show that corresponding probabilities predicted when using models G and H are very

similar—which could not be possible if the linear damping contribution were really significant for model H—confirming the beam as having almost wholly non-linear damping.

However the lower scatter in the parameters obtained for model G, would initially suggest this is the best model to use. But calibrated model H actually appears to give the best predictions compared with both the measured densities and extreme values. Therefore, upon taking into account the lack of sensitivity in the probability predictions and the evidence in the comparisons with measured data, model H is deemed superior. The predicted statistical scatter in the individual mean estimates can therefore give an unrealistically pessimistic impression of the model calibration, when in fact a reasonable level of confidence can be attached to the moment based model verification. Obviously in more general applications, to achieve a high level of confidence in the calibration of model H, a much larger sample size is needed. But an interesting general finding of the calibration, evident from Figure 11 (a–h) [and Figure 12(a–d)] is that model A (effectively an equivalent linear model) is clearly very much inferior to model H.

Finally to assess the suitability of dynamic models A–H in predicting extreme-value statistics, on the assumptions that (i) this calibration method is appropriate and (ii) a SDOF model is valid, the comparison between measured and predicted extreme value statistics shown in Figure 12(a–d) should confirm whether at least one of these assumptions is false. Indeed it is apparent from the difference between the measured positive and negative extreme values in Figure 12(a–d) that there is a small degree of vibration asymmetry. Predictions for model A are most seriously in error, but model H also shows significant disagreement, which contrasts sharply with the level of agreement found in Figure 11(h). These results show that the measured extreme values are typically more than 20% below those obtained by prediction, which translates into a probability prediction error of several orders of magnitude. Some significant effect is therefore not being taken into account. There are several possible reasons for this difference, most of which are unlikely and are ruled out shortly. These possible reasons are the following:

(1) The use of a SDOF model is inappropriate for large amplitude vibration owing to non-linear coupling and therefore a vibration model with at least two degrees-of-freedom is needed.
(2) The calibration approach is inappropriate for extreme value prediction.
(3) Predictions based on infinite bandwidth white noise might be inappropriate for systems with band-limited excitation.
(4) The Poisson assumption used in approximating extreme values might not hold.
(5) Some complex mechanism exists within the experimental rig and measuring equipment which manifests itself only at large amplitudes.

In assessing the likelihood of these reasons we can dismiss (5) because if there were some mechanism at work, one would expect some evidence in Figure 11(a–h) at large amplitude. Also it is unlikely that such a mechanism would be symmetric and therefore the difference between positive and negative extreme values should have been much more pronounced. Reasons (3) and (4) can also be dismissed since these assumptions have been examined in detail in reference [28] and found to hold for oscillators with this sort of non-linear damping. Moreover, prediction errors in Figure 12(a–d) show no dependence on duration, i.e. from $T = 1$ s to $T = 40$ s, which would otherwise be expected if this were the cause.

The possibility of inappropriate calibration of damping, can also be discounted, because the damping forces are actually greatest at some intermediate amplitudes, not at the extreme values (where damping forces are zero). Incorrect damping parameters would therefore be expected to produce visible differences in the marginal density functions particularly Figure 11(g) and 11(h).

This leaves reason (1) as the most likely cause, namely that a SDOF model is inadequate and that more degrees of freedom are needed. Note that from a measurement viewpoint (when using single point beam vibration measurements) non-linear coupling cannot be clearly observed in the displacement power spectral density because higher mode participation, described for example by using a generalized displacement model, occurs mainly at the dominant response frequency. This phenomenon is best understood in terms of coupled non-linear free vibration responses [6, 7] where higher mode participation occurs with the same period as the lowest mode (a result of non-linear coupling)—this is in contrast to free vibrations of a linear MDOF system which in general occur at distinctly different natural frequencies. The only clear way to observe non-linear coupling in forced non-linear beam vibration measurements is therefore by detailed examination of mode shape changes, as in references [14, 16]. Now the question of whether or not the level of participation suggested here, for band-limited white noise excitation of a clamped beam, compares with theoretical predictions elsewhere, there is in fact strong predicted evidence to suggest that the % higher mode participation through non-linear coupling, may indeed be very significant at normalized beam amplitudes in the range $7 < w_{\max}/r < 10$. Predictions of higher mode participation in free vibration of clamped beams are given in references [6, 7] (see Table 6 of reference [7]) and for harmonically forced vibration in reference [17]. The predicted % participation from the third mode for free vibration of beams at the lowest non-linear natural frequency is given for $w_{\max}/r \leqslant 5$ showing this to be a strongly non-linearly increasing function of $w_{\max}/r$. In fact for $w_{\max}/r = 5$ predictions show 3·2% participation from the third mode, but extrapolation to $w_{\max}/r = 10$, would give a figure around 15%. Based on such predictions it is therefore very plausible, that in forced vibration of a clamped beam with random loading there is significant non-linear coupling in the range $7 < w_{\max}/r < 10$ which is otherwise insignificant below this range. With non-central loading this coupling may involve participation from second, third and possibly higher modes. The measured extreme value results shown in Figure 12(a–d) now give great impetus to adopt a MDOF random vibration model, by using for example an FEM suggested in reference [7] or [17], to predict theoretically the level of non-linear coupling occurring in random beam vibration and to establish the model order needed for accurate extreme value prediction. The starting point for accurate forced response prediction with a reduced MDOF model however requires use of an appropriate damping model in each equation of motion of a system of coupling Duffing-type equations—our calibrated three-term model now offers distinct possibilities for meeting this requirement.

6. CONCLUSIONS

An empirical three-term non-linear damping model, for use with a single-degree-of-freedom Duffing-type equation of motion for clamped-clamped beam vibration, driven with band-limited white noise excitation, has been calibrated by using experimental measurements. Calibration has made use of a Markov moment method and finite element solutions of the stationary Fokker–Planck equation. The individual parts within the damping model are shown to have a profound effect on the accuracy of prediction, even at low level response amplitudes. Comparison between measurement and prediction by using the full calibrated model shows excellent agreement for probability density functions associated with the central beam displacement up to a normalized amplitude around $w_{\max}/r = 7$. But subsequent comparisons of measured and predicted extreme value exceedance probabilities in the range $7 < w_{\max}/r < 10$ show significant differences. Nonlinear beam coupling is identified as the most likely cause for this difference, suggesting that forced random vibrations of a clamped-clamped beam can be accurately predicted

with a SDOF model up to moderately large amplitudes, but only a little beyond this, a MDOF model is definitely needed.

REFERENCES

1. S. Woinowsky-Krieger 1950 *Journal of Applied Mechanics* **17**, 35–36. The effects of axial force on the vibration of hinged bars.
2. A. H. Nayfeh 1995 *Journal of Vibration and Control* **1**, 389–430. On direct methods for constructing nonlinear normal modes of continuous systems.
3. S. Atluri 1973 *ASME Journal of Applied Mechanics* **40**, 121–126. Nonlinear vibrations of a hinged beam including nonlinear inertia effects.
4. C. Mei 1984 *Journal of Sound and Vibration* **94**, 445–447. Comments on the Lagrange-type formulation for finite element analysis of nonlinear beam vibrations.
5. G. Singh, A. K. Sharma and G. V. Rao 1990 *Journal of Sound and Vibration* **142**(1), 77–85. Large amplitude free vibration of beams—a discussion of various formulations.
6. Y. Shi and C. Mei 1996 *Journal of Sound and Vibration* **193**(2), 453–464. A finite element time domain modal formulation for large amplitude free vibrations of beams and plates.
7. R. Y. Y. Lee, Y. Shi and C. Mei 1997 *Proceedings of the 6th International Conference on Recent Advances in Structural Dynamics*, *ISVR University of Southampton*, 1393–1407. A finite element time domain multi-mode method for large amplitude free vibrations of composite plates.
8. W. Chen, T. X. Zhong and S. P. Liang 1997 *Journal of Sound and Vibration* **206**(5), 745–748. On the DQ analysis of geometrically nonlinear vibration of immovably simply supported beams.
9. J. A. Bennet and J. G. Eisley 1970 *American Institute of Aeronautics and Astronautics* **8**, 734–739. A multiple degree of freedom approach to nonlinear beam vibrations.
10. W. Y. Tseng and J. Dugundji 1970 *Journal of Applied Mechanics* **37**, 292–297. Nonlinear vibrations of a beam under harmonic excitation.
11. C. Mei 1972 *American Institute of Aeronautics and Astronautics Journal* **10**, 292–297. Nonlinear vibrations of beams by matrix displacement method.
12. H. R. Busby and V. L. Weingarten 1973 *Journal Engineering Mechanics Division*, *ASCE* **99**, 56–68. Response of nonlinear beam to random excitation.
13. K. Takahashi 1979 *Journal of Sound and Vibration* **67**, 43–54. A method of stability analysis for nonlinear vibration of beams.
14. M. M. Bennouna and R. G. White 1984 *Journal of Sound and Vibration* **96**(3), 309–331. The effects of large vibration amplitudes on the dynamic strain response of a clamped-clamped beam with consideration of fatigue life.
15. C. Mei and K. Decha-Umphai 1985 *Journal of Sound and Vibration* **102**, 369–380. A finite element method for nonlinear forced vibration of beams.
16. R. Benamar, M. M. K. Bennouna and R. G. White 1991 *Journal of Sound and Vibration* **149**(2), 179–195. The effects of large vibration amplitudes on the mode shapes and natural frequencies of thin elastic structures—part 1: simply supported and clamped-clamped beam.
17. P. Ribeiro and M. Petyt 1997 *Proceedings of the 6th International Conference on Recent Advances in Structural Dynamics*, *ISVR University of Southampton*, 1393–1407. Nonlinear forced vibration of beams by the hierarchical finite element method.
18. A. H. Sadeghi 1991 *D.Phil. Dissertation*, *University of Sussex*. Identification and stochastic response of hysteretic systems.
19. P. W. Smith Jr, C. I. Malme and C. M. Gogos 1961 *The Journal of the Acoustical Society of America* **33**, 1476–1482. Nonlinear response of a simple clamped panel.
20. W. E. Baker, W. E. Woolam and D. Young 1967 *International Journal of Mechanical Science* **9**, 743–766. Air and internal damping of thin cantilever beams.
21. J. P. Bandstra 1981 *ASME Design Engineering Technical Conference*, *Paper No*. 81-*DET* 89. Comparison of equivalent viscous damping and nonlinear damping in discrete and continuous systems.
22. C. Mei and C. B. Prasad 1987 *Journal of Sound and Vibration* **117**(1), 173–186. Effects of nonlinear damping on random response of beams to acoustic loading.
23. C. K. Chiang 1991 *Ph.D. Dissertation*, *Old Dominion University*, *Norfolk*, *VA*. A finite element large deflection multiple-mode random response analysis of complex panels with initial stresses subjected to acoustic loading.

24. H. Wolfe 1995 *Ph.D. Dissertation*, *University of Southampton*. An experimental investigation of nonlinear behaviour of beams and plates excited to high levels of dynamic response.
25. R. R. Chen, C. Mei and H. F. Wolfe 1996 *Journal of Sound and Vibration* **195**(5), 719–738. Comparison of finite element non-linear beam random response with experimental results.
26. Y. K. Lin and G. Q. Cai 1995 *Probabilistic Structural Dynamics*. New York: Mc-Graw–Hill.
27. R. S. Langley 1985 *Journal of Sound and Vibration* **101**(1), 41–54. A finite element method for the statistics of non-linear random vibration.
28. J. F. Dunne and M. Ghanbari 1997 *Journal of Sound and Vibration* **206**(5), 697–724. Extreme-value prediction for nonlinear stochastic oscillators via numerical solutions of the stationary FPK equation.
29. A. Naess 1990 *Journal of Sound and Vibration* **138**, 365–380. Approximate first-passage and extremes of narrow-band Gaussian and non-Gaussian random vibration.
30. P. J. Gawthrop, A. Kountzeris and J. B. Roberts 1988 *Journal of Ship Research* **32**(2), 101–111. Parametric identification of nonlinear ship roll motion from forced roll data.
31. J. B. Roberts, J. F. Dunne and A. Debonos 1996 in *Advances in Non-linear Stochastic Mechanics*, 361–372. Parametric estimation for randomly excited non-linear systems. New York: Kluwer Academic.
32. B. W. Oppenheim and P. A. Wilson 1980 *Journal of Ship Research* **24**(3), 181–189. Continuous digital simulation of the second order slowly varying drift force.
33. M. Ghanbari 1996 *D.Phil. Dissertation*, *University of Sussex*. Extreme response prediction for random vibration of a clamped-clamped beam.

APPENDIX

In this appendix, application of two parameter estimation methods in their original form is demonstrated on specific SDOF clamped-clamped beam vibration model G (equation (20)) of section 5. These methods are (1) the State Variable Filter (see reference [30]), and (2) a Markov based moment method [31]. Model G is rewritten for convenience as

$$\ddot{z} + \alpha_1 \dot{z} z^2 + \alpha_2 \dot{z}|\dot{z}| + \omega_n^2 z + \gamma \omega_n^2 z^3 = Aw(t),$$

where the excitation is modelled as a standard Gaussian white noise process $w(t)$ with intensity A. The parameter estimation problem, simply stated is: how do you obtain accurate parameter values from measurements of system input–output behaviour? In general this requires explicit excitation and response information, but in particular situations, parameter estimation may be possible using only partial information. The state variable filter does in fact require explicit force and response measurements but is in fact very general; the Markov moment method can be exploited without explicit excitation time histories when this is assumed to be white noise. Application of both of these 'linear-in-the-parameter' estimation methods is now demonstrated:

A.1. THE STATE VARIABLE FILTER PARAMETER ESTIMATION METHOD (SVF)

Consider equation (20) expressed in more general form as

$$\ddot{z} + \alpha_1 \dot{z} z^2 + \alpha_2 \dot{z}|\dot{z}| + \omega_n^2 z + \gamma \omega_n^2 z^3 = bf(t), \tag{A1}$$

where now the excitation $f(t)$ can be any continuous function provided it is sufficiently 'rich' containing at least two different excitation frequencies. To implement the SVF, the terms $m_1 \dot{z}$ and $m_2 z$ are initially added to both sides of equation (A1):

$$\ddot{z} + m_1 \dot{z} + m_2 z = m_1 \dot{z} + m_2 z - \alpha_1 z z^2 - \alpha_2 \dot{z}|\dot{z}| - \omega_n^2 z^3 - \gamma \omega_n^2 z^3 + bf(t).$$

Then two terms are defined;

$$f_1 = -m_1, \qquad f_2 = \omega_n^2 - m_2, \tag{A2, A3}$$

where m_1 and m_2 are constant value filter coefficients (chosen *a priori* largely by trial and error); then on rearranging, equation (A2) becomes

$$\ddot{z} + m_1 z + m_2 z = -f_1 \dot{z} - \alpha_1 \dot{z} z^2 - \alpha_2 \dot{z}|\dot{z}| - f_2 z - \gamma \omega_n^2 z^3 + bf(t). \tag{A4}$$

Equation (A4) represents the linear state-variable filter, in which the coefficients to be estimated, appear on the right-hand side. One can introduce the following set of 'auxiliary' equations:

$$\frac{d^2}{dt^2}(y_1) + m_1 \frac{d}{dt}(y_1) + m_2(y_1) = -z(t) \tag{A5}$$

$$\frac{d^2}{dt^2}(y_2) + m_1 \frac{d}{dt}(y_2) + m_2(y_2) = -\dot{z}(t) z^2(t) \tag{A6}$$

$$\frac{d^2}{dt^2}(y_3) + m_1 \frac{d}{dt}(y_3) + m_2(y_3) = -\dot{z}(t)|\dot{z}(t)| \tag{A7}$$

$$\frac{d^2}{dt^2}(y_4) + m_1 \frac{d}{dt}(y_4) + m_2(y_4) = -z^3(t) \tag{A8}$$

$$\frac{d^2}{dt^2}(y_5) + m_1 \frac{d}{dt}(y_5) + m_2(y_5) = f(t), \tag{A9}$$

Upon multiplying equation (A5) by f_2, one has

$$\frac{d^2}{dt^2}(f_2 y_1) + m_1 \frac{d}{dt}(f_2 y_1) + m_2(f_2 y_1) = -f_2 z(t), \tag{A10}$$

and then differentiating equation (A5) and multiplying by f_1 one obtains

$$\frac{d^2}{dt^2}(f_1 \dot{y}_1) + m_1 \frac{d}{dt}(f_1 \dot{y}_1) + m_2(f_1 \dot{y}_1) = -f_1 \dot{z}(t). \tag{A11}$$

Upon multiplying equation (A6) by α_1 it follows that

$$\frac{d^2}{dt^2}(\alpha_1 y_2) + m_1 \frac{d}{dt}(\alpha_1 y_2) + m_2(\alpha_1 y_2) = -\alpha_1 \dot{z}(t) z^2(t), \tag{A12}$$

and multiplying equation (A7) by α_2 one obtains

$$\frac{d^2}{dt^2}(\alpha_2 y_3) + m_1 \frac{d}{dt}(\alpha_2 y_3) + m_2(\alpha_2 y_3) = -\alpha_2 \dot{z}(t)|\dot{z}(t)|. \tag{A13}$$

Then multiplying equation (A8) by $\gamma \omega_n^2$ gives

$$\frac{d^2}{dt^2}(\gamma \omega_n^2 y_4) + m_1 \frac{d}{dt}(\gamma \omega_n^2 y_4) + m_2(\gamma \omega_n^2 y_4) = -\gamma \omega_n^2 z^3(t), \tag{A14}$$

and finally multiplying equation (A9) by b one obtains

$$\frac{d^2}{dt^2}(b y_5) + m_1 \frac{d}{dt}(b y_5) + m_2(b y_5) = bf(t). \tag{A15}$$

Adding equation (A10) to (A15) gives, on comparison with equation (A4), the following equality of variables:

$$z = f_1 \dot{y}_1 + f_2 y_1 + \alpha_1 y_2 + \alpha_2 y_3 + \gamma \omega_n^2 y_4 + b y_5. \tag{A16}$$

On introducing state vector notation and letting

$$\underline{U}(t) = \begin{bmatrix} \dot{y}_1 \\ y_1 \\ y_2 \\ y_3 \\ y_4 \\ y_5 \end{bmatrix}, \qquad \underline{\theta} = \begin{bmatrix} f_1 \\ f_2 \\ \alpha_1 \\ \alpha_2 \\ \gamma\omega_n^2 \\ b \end{bmatrix},$$

one can then write equation (A16) compactly as

$$z(t) = \underline{U}^{\mathrm{T}}(t)\underline{\theta} \tag{A17}$$

(where the superscript T denotes the transpose). $\underline{U}(t)$ is known as the estimation filter state, and $\underline{\theta}$ is the parameter vector. Since in practice $z(t)$ is measured at times $t_i = i \times \Delta t$ (Δt is the sampling time interval), equation (A17) can be modified to

$$z_i(t_i) = \underline{U}^{\mathrm{T}}(t_i)\underline{\theta}, \tag{A18}$$

and the error equation is written as

$$E = z(t_i) - \underline{U}^{\mathrm{T}}(t_i)\underline{\theta}. \tag{A19}$$

Estimates of the parameter vector $\underline{\theta}$ can be obtained by minimizing the error equation (A19) (in a least-square sense) where the summed square error is

$$J = \sum_{i=0}^{N} [z(t_i) - \underline{U}^{\mathrm{T}}(t_i)\underline{\theta}]^2. \tag{A20}$$

Off-line (non-recursive) algorithms can be used to estimate the parameter vector $\underline{\theta}$, which minimizes the cost function J. Alternatively parameter estimation may proceed recursively by marching forward in time, allowing the evolution of the parameters to be studied. The recursive algorithm used here is summarized as follows:

If we let $\underline{\hat{\theta}}_N$ be the least square estimate of $\underline{\theta}$ at time $t_i = i \times \Delta t$ and $\underline{U}_i = \underline{U}(t = t_i)$, $z_i = z(t = t_i)$ and also let

$$\underline{S}_N = \sum_{i=0}^{N} \underline{U}_i \underline{U}_i^{\mathrm{T}}, \tag{A21}$$

then at corresponding time t_n, the algorithm can be written in five steps (a)–(e) by using appropriate variables as follows:

(a) $$\sigma_{N+1} = \underline{U}_{N+1}^{\mathrm{T}} \underline{S}_N^{-1} \underline{U}_{N+1}, \tag{A22}$$

(b) $$\underline{K}_{N+1} = \frac{1}{(1 + \sigma_{N+1})} \underline{S}_N^{-1} \underline{U}_{N+1}, \tag{A23}$$

(c) $$\hat{e}_{N+1} = z_{N+1} - \underline{U}_{N+1}^{\mathrm{T}} \underline{\hat{\theta}}_N, \tag{A24}$$

(d) $$\underline{\hat{\theta}}_{N+1} = \underline{\hat{\theta}} + \underline{K}_{N+1} \hat{e}_{N+1} \tag{A25}$$

(e) $$\underline{S}_{N+1}^{-1} = \underline{S}_N^{-1} - (1 + \sigma_{N+1}) \underline{K}_{N+1} \underline{K}_{N+1}^{\mathrm{T}}. \tag{A26}$$

Steps (a) to (e) can be repeated at times t_{N+1} and so on, enabling $\underline{\hat{\theta}}_N$ to be evaluated recursively. To start this algorithm, it is necessary to specify initial values for $\underline{\theta}$ and $\underline{S}_{-1}^{-1}$

at time zero. In practice these are chosen as $\hat{\underline{\theta}}_{-1} = \underline{0}$, $\underline{S}_{-1}^{-1} = \lambda \underline{I}$, where $\underline{I}$ is the unit matrix and λ is a large scalar, typically chosen around 10^5.

A.2. MOMENT BASED PARAMETER ESTIMATION USING MARKOV PROCESS THEORY

The SVF method described above requires explicit, measurements of both excitation and response processes—in this alternative approach Markov process theory [31] is used to construct a system of equations which the response moments and the parameters must satisfy. This is particularly suited to systems driven by broad-band noise where only moments of the response process are known. Again this method is implemented for estimation of parameters in model G [equation (20)]. When equation (20) is put into random differential (Îto) form,

$$\dot{\underline{z}} = \underline{g}(\underline{z}) + G\underline{w}(t) \tag{A27}$$

where the vectors $\underline{z}$ and $\dot{\underline{z}}$ (the response and velocity) constitute an n dimensional vector Markov process. Here $\underline{w}(t)$ is a zero mean uncorrelated vector of Gaussian white noise processes with constant spectral density of unit amplitude; $\underline{g}(\underline{z})$ is a vector of system functions.

The general form of the FPK equation associated with equation (A27) is

$$\frac{\partial p(\underline{z})}{\partial t} = -\sum_{i=1}^{n} \frac{\partial}{\partial z_i}[g_i(\underline{z})p(\underline{z})] + \frac{1}{2}\sum_{i=1}^{n}\sum_{j=1}^{n} B_{ij}\frac{\partial^2}{\partial z_i\,\partial z_j}[p(\underline{z})], \tag{A28}$$

where $B = 2\pi GG^{\mathrm{T}}$ and $p(\underline{z})$ is the joint probability density function of the system.

Moment differential equations associated with equation (A28) can be written as

$$\frac{d}{dt}E(h) = \sum_{i=1}^{n} E\left(g_i\frac{\partial h}{\partial z_i}\right) + \frac{1}{2}\sum_{i=1}^{n}\sum_{j=1}^{n} E\left(B_{ij}\frac{\partial^2 h}{\partial z_i \partial z_j}\right) + E\left(\frac{\partial h}{\partial t}\right), \tag{A29}$$

where the function $h(\underline{z}, t) = z_1^{k_1} z_2^{k_2} \cdots z_n^{k_n}$. Application of the expectation operator produces moments $E(h) = E(z_1^{k_1} z_2^{k_2} \cdots z_n^{k_n})$. From equation (A29), explicit sets of moment differential equations of different orders $(k_1 + k_2)$ can be established and when the individual moments are known, the hierarchy of moment equations can be truncated to give a set of equations satisfied by unknown parameters. Application of this approach to equation (20) gives the corresponding moment differential equations:

$$\begin{aligned}\dot{E}(z_1^{k_1} z_2^{k_2}) = {} & k_1 E(z_1^{k_1-1} z_2^{k_2+1}) - k_2 E[(\alpha_1 z_2 z_1^2 + \alpha_2 z_2|z_2|)(z_1^{k_1} z_2^{k_2-1})] \\ & - k_2 E[(\omega_n^2 z_1 + \gamma\omega_n^2 z_1^3)(z_1^{k_1} z_2^{k_2-1})] + \pi A^2 k_2(k_2-1)E(z_1^{k_1} z_2^{k_2-2}).\end{aligned} \tag{A30}$$

These are non-stationary moments which can be difficult to use with stationary data. However stationary moments can also be used directly by assuming that $\dot{E}(z_1^{k_1} z_1^{k_2}) = 0$. Moreover, a property of stationary stochastic processes, gives zero odd moments; i.e. $E(z_1^{k_1} z_2^{k_2}) = 0$ for $k_1 + k_2 = 2{*}k + 1$ where $k = 0, 1, 2, \ldots$. In addition, for symmetric joint probability density functions it can shown that the following expectations are also zero: $E(z_1^{k_1} z_2) = E(z_1^{k_1} z_2|z_2|) = 0$ for $k_1 = 2k + 1$, where $k = 0, 1, 2, 3, \ldots$. Upon taking account of these properties, as applied to model G for example, an exact set of stationary moment equations can be constructed. Here, the second, fourth, sixth and eighth orders are written out explicitly for the appropriate combinations of k_1 and k_2 forming a set

of 20 equations, from which the unknown parameters α_1, α_2, ω_n^2 and $\gamma\omega_n^2$ could in principle be estimated:

second order: [e.g. combination with $k_1 + k_2 = 2$, k_1 always indexed from zero i.e. $(k_1, k_2) = (0, 2); (1, 1)$]

$$k_2[\alpha_1 E(z_1^2 z_2^2) + \alpha_2 E(z_2^2|z_2|) + \omega_n^2 E(z_1 z_2) + \gamma\omega_n^2 E(z_1^3 z_2)] = \pi A^2 k_2(k_2 - 1), \tag{A31}$$

$$k_2[\alpha_1 E(z_1^3 z_2) + \alpha_2 E(z_1 z_2|z_2|) + \omega_n^2 E(z_1^2) + \gamma\omega_n^2 E(z_1^4)] = k_1 E(z_2^2); \tag{A32}$$

fourth order: [combination with $k_1 + k_2 = 4$, $(k_1, k_2) = (0, 4); (1, 3); (2,2); (3, 1)$]

$$k_2[\alpha_1 E(z_2^4) + \alpha_2 E(z_2^4|z_2|) + \omega_n^2 E(z_1 z_2^3) + \gamma\omega_n^2 E(z_1^3 z_3^3)] = \pi A^2 k_2(k_2 - 1) E(z_2^2), \tag{A33}$$

$$k_2[\alpha_1 E(z_1^3 z_2^3) + \alpha_2 E(z_1 z_2^4|z_2|) + \omega_n^2 E(z_1^2 z_2^2) + \gamma\omega_n^2 E(z_1^4 z_2^2)] = \pi A^2 k_2(k_2 - 1) E(z_1 z_2) + k_1 E(z_2^4), \tag{A34}$$

$$k_2[\alpha_1 E(z_1^4 z_2^2) + \alpha_2 E(z_1^2 z_2^2|z_2|) + \omega_n^2 E(z_1^3 z_2) + \gamma\omega_n^2 E(z_1^5 z_1)] = \pi A^2 k_2(k_2 - 1) E(z_1^2) + k_1 E(z_1 z_2^3), \tag{A35}$$

$$k_2[\alpha_1 E(z_1^5 z_2) + \alpha_2 E(z_1^3 z_2|z_2|) + \omega_n^2 E(z_1^4) + \gamma\omega_n^2 E(z_1^6)] = k_1 E(z_1^2 z_2^2); \tag{A36}$$

sixth order:

$$k_2[\alpha_1 E(z_1^2 z_2^6) + \alpha_2 E(z_2^6|z_2|) + \omega_n^2 E(z_1^1 z_2^5) + \gamma\omega_n^2 E(z_1^3 z_2^5)] = \pi A^2 k_2(k_2 - 1) E(z_2^4), \tag{A37}$$

$$k_2[\alpha_1 E(z_1^3 z_2^5) + \alpha_2 E(z_1 z_2^5|z_2|) + \omega_n^2 E(z_1^2 z_2^4) + \gamma\omega_n^2 E(z_1^4 z_2^4)] = \pi A^2 k_2(k_2 - 1) E(z_1 z_2^3) + k_1 E(z_2^6), \tag{A38}$$

$$k_2[\alpha_1 E(z_1^4 z_2^4) + \alpha_2 E(z_1^2 z_2^4|z_2|) + \omega_n^2 E(z_1^3 z_2^3) + \gamma\omega_n^2 E(z_1^5 z_2^3)] = \pi A^2 k_2(k_2 - 1) E(z_1^2 z_2^2) + k_1 E(z_1 z_2^5), \tag{A39}$$

$$k_2[\alpha_1 E(z_1^5 z_2^3) + \alpha_2 E(z_1^3 z_2^3|z_2|) + \omega_n^2 E(z_1^4 z_2^2) + \gamma\omega_n^2 E(z_1^6 z_2^2)] = \pi A^2 k_2(k_2 - 1) E(z_1^3 z_2) + k_1 E(z_1^2 z_2^4), \tag{A40}$$

$$k_2[\alpha_1 E(z_1^6 z_2^2) + \alpha_2 E(z_1^4 z_2^2|z_2|) + \omega_n^2 E(z_1^5 z_2) + \gamma\omega_n^2 E(z_1^7 z_1)] = \pi A^2 k_2(k_2 - 1) E(z_1^4) + k_1 E(z_1^3 z_2^3), \tag{A41}$$

$$k_2[\alpha_1 E(z_1^7 z_2) + \alpha_2 E(z_1^5 z_2|z_2|) + \omega_n^2 E(z_1^6) + \gamma\omega_n^2 E(z_1^8)] = k_1 E(z_1^4 z_2^2); \tag{A42}$$

eighth order:

$$k_2[\alpha_1 E(z_1^2 z_2^8) + \alpha_2 E(z_2^8|z_2|) + \omega_n^2 E(z_1 z_2^7) + \gamma\omega_n^2 E(z_1^3 z_2^7)] = \pi A^2 k_2(k_2 - 1) E(z_2^6), \tag{A43}$$

$$k_2[\alpha_1 E(z_1^3 z_2^7) + \alpha_2 E(z_1 z_2^7|z_2|) + \omega_n^2 E(z_1^2 z_2^6) + \gamma\omega_n^2 E(z_1^4 z_2^6)] = \pi A^2 k_2(k_2 - 1) E(z_1 z_2^5) + k_1 E(z_2^8), \tag{A44}$$

$$k_2[\alpha_1 E(z_1^4 z_2^6) + \alpha_2 E(z_1^2 z_2^6|z_2|) + \omega_n^2 E(z_1^3 z_2^5) + \gamma\omega_n^2 E(z_1^5 z_2^5)] = \pi A^2 k_2(k_2 - 1) E(z_1^2 z_2^4) + k_1 E(z_1 z_2^7), \tag{A45}$$

$$k_2[\alpha_1 E(z_1^5 z_2^5) + \alpha_2 E(z_1^3 z_2^5|z_2|) + \omega_n^2 E(z_1^4 z_2^4) + \gamma\omega_n^2 E(z_1^6 z_2^4)] = \pi A^2 k_2(k_2 - 1) E(z_1^3 z_2^3) + k_1 E(z_1^2 z_2^6), \tag{A46}$$

$$k_2[\alpha_1 E(z_1^6 z_2^4) + \alpha_2 E(z_1^4 z_2^4|z_2|) + \omega_n^2 E(z_1^5 z_2^3) + \gamma\omega_n^2 E(z_1^7 z_2^3)] = \pi A^2 k_2(k_2 - 1) E(z_1^4 z_2^2) + k_1 E(z_1^3 z_2^5), \tag{A47}$$

$$k_2[\alpha_1 E(z_1^7 z_2^3) + \alpha_2 E(z_1^5 z_2^3|z_2|) + \omega_n^2 E(z_1^6 z_2^2) + \gamma\omega_n^2 E(z_1^8 z_2^2)]$$
$$= \pi A^2 k_2(k_2 - 1)E(z_1^5 z_2) + k_1 E(z_1^4 z_2^4), \tag{A48}$$

$$k_2[\alpha_1 E(z_1^8 z_2^2) + \alpha_2 E(z_1^6 z_2^2|z_2|) + \omega_n^2 E(z_1^7 z_2) + \gamma\omega_n^2 E(z_1^9 z_2)]$$
$$= \pi A^2 k_2(k_2 - 1)E(z_1^6) + k_1 E(z_1^5 z_2^3), \tag{A49}$$

$$k_2[\alpha_1 E(z_1^9 z_2) + \alpha_2 E(z_1^7 z_2|z_2|) + \omega_n^2 E(z_1^8) + \gamma\omega_n^2 E(z_1^{10})] = k_1 E(z_1^6 z_2^2). \tag{A50}$$

But an examination of the absolute magnitudes of several mixed moment estimates allows them to be ignored, namely $E(z_1 z_2^3)$, $E(z_1 z_2^3|z_2|)$, $E(z_1^3 z_2^3)$, $E(z_1^3 z_2^3|z_2|)$, $E(z_1 z_2^5)$, $E(z_1 z_2^5|z_2|)$, $E(z_1^5 z_2^3)$, $E(z_1^3 z_2^5)$ since these are typically very much smaller than other moments (by a factor of at least 1000). A simplified set of second to eighth order moment equations can therefore be written for model G as follows:
second order:

$$k_2[\alpha_1 E(z_1^2 z_2^2) + \alpha_2 E(z_2^2|z_2|)] = \pi A^2 k_2(k_2 - 1), \tag{A51}$$

$$k_2[\omega_n^2 E(z_1^2) + \gamma\omega_n^2 E(z_1^4)] = k_1 E(z_2^2); \tag{A52}$$

fourth order:

$$k_2[\alpha_1 E(z_2^4) + \alpha_2 E(z_2^4|z_2|)] = \pi A^2 k_2(k_2 - 1)E(z_2^2), \tag{A53}$$

$$k_2[\omega_n^2 E(z_1^2 z_2^2) + \gamma\omega_n^2 E(z_1^4 z_2^2)] = k_1 E(z_2^4), \tag{A54}$$

$$k_2[\alpha_1 E(z_1^4 z_2^2) + \alpha_2 E(z_1^2 z_2^2|z_2|)] = \pi A^2 k_2(k_2 - 1)E(z_1^2), \tag{A55}$$

$$k_2[\omega_n^2 E(z_1^4) + \gamma\omega_n^2 E(z_1^6)] = k_1 E(z_1^2 z_2^2); \tag{A56}$$

sixth order:

$$k_2[\alpha_1 E(z_1^2 z_2^6) + \alpha_2 E(z_2^6|z_2|)] = \pi A^2 k_2(k_2 - 1)E(z_2^4), \tag{A57}$$

$$k_2[\omega_n^2 E(z_1^2 z_2^4) + \gamma\omega_n^2 E(z_1^4 z_2^4)] = \pi A^2 k_2(k_2 - 1)E(z_1 z_2^3) + k_1 E(z_2^6), \tag{A58}$$

$$k_2[\alpha_1 E(z_1^4 z_2^4) + \alpha_2 E(z_1^2 z_2^4|z_2|)] = \pi A^2 k_2(k_2 - 1)E(z_1^2 z_2^2), \tag{A59}$$

$$k_2[\omega_n^2 E(z_1^4 z_2^2) + \gamma\omega_n^2 E(z_1^6 z_2^2)] = k_1 E(z_1^2 z_2^4), \tag{A60}$$

$$k_2[\alpha_1 E(z_1^6 z_2^2) + \alpha_2 E(z_1^4 z_2^2|z_2|)] = \pi A^2 k_2(k_2 - 1)E(z_1^4), \tag{A61}$$

$$k_2[\omega_n^2 E(z_1^6) + \gamma\omega_n^2 E(z_1^8)] = k_1 E(z_1^4 z_2^2); \tag{A62}$$

eighth order:

$$k_2[\alpha_1 E(z_1^2 z_2^8) + \alpha_2 E(z_2^8|z_2|)] = \pi A^2 k_2(k_2 - 1)E(z_2^6), \tag{A63}$$

$$k_2[\omega_n^2 E(z_1^2 z_2^6) + \gamma\omega_n^2 E(z_1^4 z_2^6)] = k_1 E(z_2^8), \tag{A64}$$

$$k_2[\alpha_1 E(z_1^4 z_2^6) + \alpha_2 E(z_1^2 z_2^6|z_2|)] = \pi A^2 k_2(k_2 - 1)E(z_1^2 z_2^4), \tag{A65}$$

$$k_2[\omega_n^2 E(z_1^4 z_2^4) + \gamma\omega_n^2 E(z_1^6 z_2^4)] = k_1 E(z_1^2 z_2^6), \tag{A66}$$

$$k_2[\alpha_1 E(z_1^6 z_2^4) + \alpha_2 E(z_1^4 z_2^4|z_2|)] = \pi A^2 k_2(k_2 - 1)E(z_1^4 z_2^2), \tag{A67}$$

$$k_2[\omega_n^2 E(z_1^6 z_2^2) + \gamma\omega_n^2 E(z_1^8 z_2^2)] = k_1 E(z_1^4 z_2^4), \tag{A68}$$

$$k_2[\alpha_1 E(z_1^8 z_2^2) + \alpha_2 E(z_1^6 z_2^2|z_2|)] = \pi A^2 k_2(k_2 - 1)E(z_1^6), \tag{A69}$$

$$k_2[\omega_n^2 E(z_1^8) + \gamma\omega_n^2 E(z_1^{10})] = k_1 E(z_1^6 z_2^2). \tag{A70}$$

Equations (A51)–(A70) now constitute a set of equations from which damping and stiffness parameters can be estimated, where the required expectations are replaced by sample moments obtained from measured response data. Note that use of more equations than unknowns, allows a least square error solution to be found [31].

It is evident from this (reduced) set of equations, that particular equations containing stiffness parameters are uncoupled from those in which damping terms appear (a consequence of the simplifications made earlier). Even numbered equations (A52)–(A70) therefore contain only stiffness parameters ω_n^2 and $\gamma\omega_n^2$—consequently simultaneous solution of at least any two of these equations will yield explicit stiffness parameter estimates. To obtain estimates of the damping parameters, it is evident that the odd numbered equations (A51)–(A69) contain only parameters α_1 and α_2, but it is important to note that the right hand side of each equation includes the excitation intensity term A^2. When the excitation intensity is known then explicit parameters can indeed be readily obtained. But when the excitation intensity is not known, damping parameters can only be obtained in terms of ratios involving A^2. But if the parameters are to be directly used for prediction in the FPK equation (namely at the same excitation level as measured data), then use of the raw damping-to-intensity ratios (along with explicit stiffness parameters) is sufficient to be able to make a corresponding prediction. This can be demonstrated by direct substitution into the FPK equation, of the stiffness and damping parameters, $\alpha_1 A^2$, $\alpha_2 A^2$, ω_n^2 and $\gamma\omega_n^2$, as follows:

$$\pi A^2 \frac{\partial^2 p}{\partial z_2^2} - \frac{\partial (z_2 p)}{\partial z_1} + \frac{\partial}{\partial z_2}\left[\{\alpha_1 A^2 z_2 z_1^2 + \alpha_2 A^2 |\dot{z}_2|\dot{z}_2 + \omega_n^2 z_1 + \omega_n^2 \gamma z_1^3\} p\right] = 0. \tag{A71}$$

Now to show (by example) that the probability density function is independent of intensity level A, write the corresponding stationary moment equations (A30) associated with FPK equation (A71) in the form

$$-k_1 E(z_1^{k_1-1} z_2^{k_2+1}) + k_2 E[(\alpha_1 A^2 z_2 z_1^2 + \alpha_2 A^2 z_2 |z_2|)(z_1^{k_1} z_2^{k_2-1})]$$
$$+ k_2 E[(\omega_n^2 z_1 + \gamma\omega_n^2 z_1^3)(z_1^{k_1} z_2^{k_2})] = \pi A^2 k_2 (k_2 - 1) E(z_1^{k_1} z_2^{k_2-2}) = 0. \tag{A72}$$

It can be seen, for example, that a moment equation, say for the particular case, $k_1 = 0$ and $k_2 = 2$ can be written as

$$k_2[\alpha_1 A^2 E(z_1^2 z_2^2) + \alpha_2 A^2 E(z_2^2 |z_2|) + \omega_n^2 E(z_1 z_2) + \gamma\omega_n^2 E(z_1^3 z_2)] = \pi A^2 k_2 (k_2 - 1). \tag{A73}$$

It is assumed that all moments in equation (A73), except $E(z_1^2 z_2^2)$, are known exactly, then on rearranging this gives

$$[E(z_1^2 z_2^2)] = \frac{\pi A^2 (k_2 - 1) - \alpha_2 A^2 E(z_2^2 |z_2|) - \omega_n^2 E(z_1 z_2) - \gamma\omega_n^2 E(z_1^3 z_2)}{\alpha_1 A^2}. \tag{A74}$$

Equation (A74) demonstrates that to find $E(z_1^2 z_2^2)$, the intensity level A must in general be known. But since certain moments, such as $E(z_1 z_2)$ and $E(z_1^3 z_2)$ can be ignored since they are either zero or are very small in comparison with other moments, equation (A74) can be rewritten as

$$[E(z_1^2 z_2^2)] = \frac{\pi(k_2 - 1) - \alpha_2 E(z_2^2 |z_2|)}{\alpha_1}. \tag{A75}$$

Upon applying the same argument to all other appropriate moments in equation (A73), it can be seen that these too are largely independent of the intensity level A.

Finally solution of appropriate sets of equations (A51)–(A70) have been implemented in sections 3 and 5 to generate empirical evidence to suggest the best sets of moment equations to use, namely the set of second, fourth and sixth order equations. Finally to provide least square error solutions to these (oversubscribed) equations, NAG library routine E04FCF has been used.